

# 1 **Pain-related learning signals in the human insula**

2 Björn Horing\* & Christian Büchel

3 Affective Neuroscience Group, Department of Systems Neuroscience, University Medical Center Hamburg-Eppendorf,

4 22303 Hamburg, Germany

5 \*Corresponding author, e-mail [b.horing@uke.de](mailto:b.horing@uke.de)

6

## 7 Abstract

8 Pain is not only a perceptual phenomenon, but also a preeminent learning signal. In reinforcement learning models,  
9 prediction errors (PEs) play a crucial role, i.e. the mismatch between expectation and sensory input. In particular,  
10 advanced learning models require the representation of different types of PEs, namely signed PEs (whether more or less  
11 pain was expected) to specify the direction of learning, and unsigned PEs (the absolute deviation from an expectation) to  
12 adapt the learning rate. The insula has been shown to play an important role in pain intensity coding and in signaling  
13 surprise. However, mainly unsigned PEs could be identified in the anterior insula. It remains an open question whether  
14 these PEs are specific to pain, and whether signed PEs are also represented in the insula.

15 To answer these questions, 47 subjects learned associations of two conditioned stimuli (CS) with four unconditioned  
16 stimuli (US; painful heat or loud sound, of one low and one high intensity each) while undergoing functional magnetic  
17 resonance imaging (fMRI) and skin conductance response (SCR) measurements. CS-US associations reversed multiple  
18 times between intensities and between sensory modalities, generating frequent PEs.

19 SCRs indicated comparable nonspecific characteristics of the two modalities. fMRI analyses focusing on the insular and  
20 opercular cortices contralateral to painful stimulation showed that activation in the anterior insula correlated with  
21 unsigned intensity PEs. Importantly, this unsigned PE signal was similar for pain and aversive sounds and also modality  
22 PEs, indicating an unspecific aversive surprise signal. Conversely, signed pain intensity PE signals were modality-specific  
23 and located in the dorsal posterior insula, an area previously implicated in pain intensity processing.

24 Previous studies have identified abnormal insula function and abnormal learning as potential causes of pain  
25 chronification. Our findings link these results and suggest one potential mechanism, namely a misrepresentation of  
26 learning relevant prediction errors in the insular cortex.

## 27 Introduction

28 Apart from its role in signaling tissue damage, pain is increasingly considered to be a preeminent teaching signal [1,2] in  
29 the context of reinforcement learning models [3]. For example, delta rule learning models in classical fear conditioning,  
30 such as the Rescorla-Wagner model [4], almost exclusively employ pain as unconditioned stimulus (US). In this and  
31 similar models, the value of predictive cues (conditioned stimuli, CS) is updated by the difference between the expected  
32 and the experienced outcome, i.e. a prediction error (PE). In this case the PE needs to be *signed* and signals the direction  
33 of the difference between expectation and event, i.e. whether the outcome is better or worse than expected. In the case  
34 of an aversive event like painful stimulation, this is relevant for shaping future behavior. Reinforcement learning  
35 particularly relies on these valences, and different neuronal correlates have been reported for aversive compared to  
36 appetitive PEs [5–8]. This has important clinical implications, as pathological learning mechanisms [1,9] have been  
37 reported in chronic pain.

38 However, PEs can also be computed as *unsigned* [10–12]. An unsigned PE simply indicates the presence of an  
39 unexpected event regardless of its valence. Unsigned PEs are therefore conceptually related to constructs like surprise  
40 or salience, and may contain information concerning the urgency of behavioral change [13]. Computational models of  
41 learning can include either type of PE, or both [4,10,14–16] – for example, the Pearce-Hall model incorporates the  
42 unsigned PE as a factor to increase the learning rate after highly incongruent (surprising) events [14,17], whereas a  
43 hybrid-model contains both terms [10,17,18].

44 Previous studies investigating PEs in the context of aversive learning have observed signal changes in the anterior insula  
45 related to unsigned PEs [6,12,19–21]. Unfortunately, in many studies, a signed PE signal is non-orthogonal to stimulus  
46 expectation, which poses a problem with a short interval between CS and US, and the low temporal resolution of  
47 functional magnetic resonance imaging (fMRI). Consequently, these studies were suboptimal to investigate signed PEs.

48 Granted that unsigned PEs resemble a surprise signal, they could plausibly involve similar regions for all surprising  
49 events, independent of the stimulus sensory modality. Crucially, the representation of unsigned pain PEs in the anterior  
50 insula [12,19] raises the question of whether these are specific to pain, or simply related to aversive events.

51 To further investigate the existence of signed PEs and the modality-specificity of unsigned PEs, as well as the underlying  
52 neuronal mechanisms, we used a Pavlovian transreinforcer reversal learning paradigm [22,23]. This involves two visual  
53 stimuli as CS, and two intensities of painful heat or loud sounds as US (for brevity, these are referred to as “pain” and  
54 “sound” forthwith). Across sensory modalities, stimuli were chosen to be roughly comparable in salience as indicated by  
55 similar skin conductance responses (SCR) [24]. Reversals occurred between US intensity but within US modality (e.g. CS  
56 predicting low pain will next predict high pain), or within US intensity but between US modality (e.g. CS predicting loud

57 sound will next predict high pain). Analyses focused on PEs within and across modalities, using advanced surface based  
58 analyses of high resolution fMRI together with skin conductance responses.

59 We expected that SCR resembles unsigned PEs, as SCR is generally considered to reflect arousal-related activation [25–  
60 27] and thus the sign of the PE – representing its valence – should not affect it. Concerning fMRI, we expected to  
61 replicate previous results [12,19] showing the representation of unsigned PEs in the anterior insula. More importantly,  
62 we expected that this signal occurs independent of the modality of the US (i.e. both for sound and pain). In agreement  
63 with this nonspecific response, we also expected modality PEs to be represented in the anterior insula. However, in this  
64 case we expected a weaker signal, as the intensity – and thus salience and other general aspects – are intendedly not  
65 different between the expected and the received US.

66 Employing our novel paradigm, we were also in the position to investigate signed intensity PEs. Focusing on pain, we  
67 expected them to be either represented as a distinct part of the anterior insula, or within the mid to posterior insula.  
68 The former is suggested by inherent differences in salience between the two intensities, the latter by the notion that a  
69 signed PE necessitates some form of intensity encoding, which has been observed in the dorsal posterior insula [24,28–  
70 30].

## Results

In two sessions with 64 trials each, 47 subjects learned associations of two conditioned stimuli (fractal pictures; CS) with individually calibrated unconditioned stimuli (US; two painful heat intensities and two loud sound intensities) (Figure 1a, b). In each trial, either CS appeared, followed by symbols of all four US, from which subjects selected the US they expected (Figure 1c). One of the US was then applied. CS/US associations were deterministic, but importantly, associations frequently reversed and had to be relearned over the course of the experiment (Figure 2). Reversals occurred unannounced after a randomized number of trials. Reversals could occur along the modality dimension or the intensity dimension, but not both simultaneously (e.g., no low heat to high sound reversals). See Materials and Methods and Supporting Figure 1 for further details concerning design and protocol.

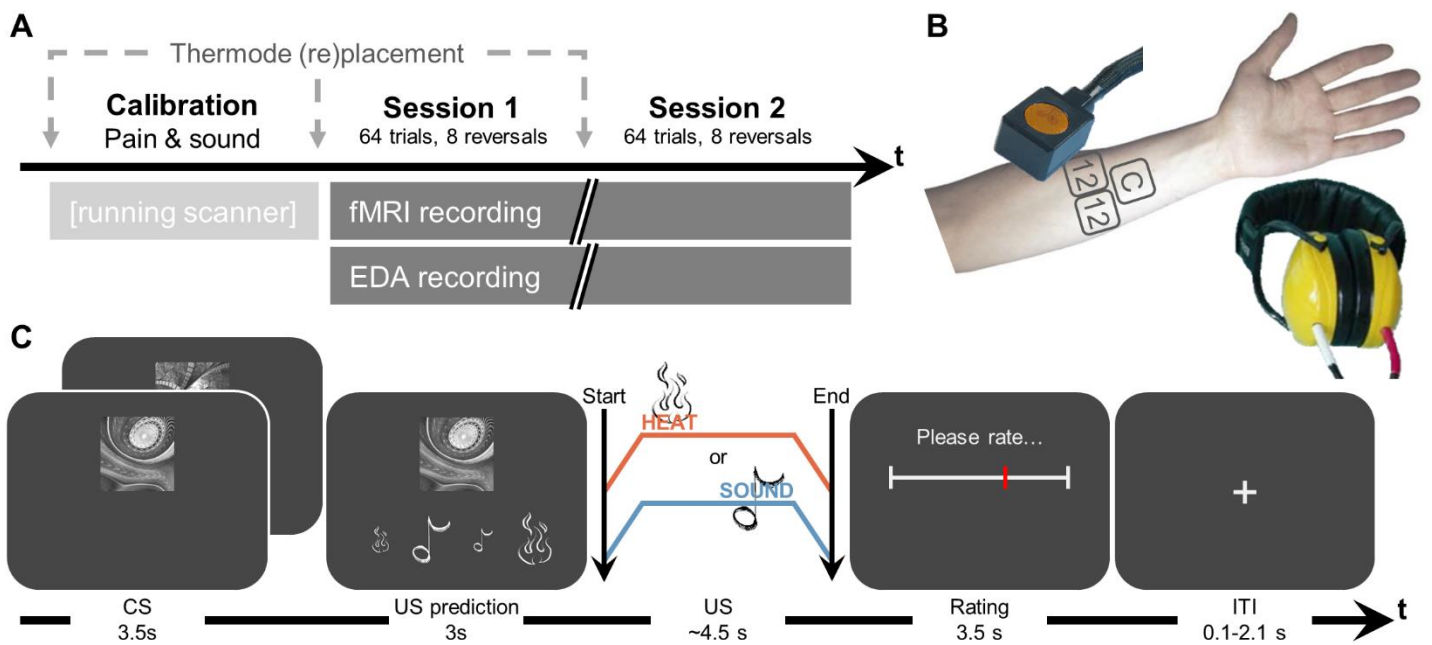


**Figure 1.** Experimental protocol. **(A)** Overall structure of the experiment. Calibration took ~15 minutes, each session ~20 minutes. **(B)** Devices used for heat stimulation (thermode) and sound stimulation (headphones), with standardized locations on the left arm for pain calibration and either of the two experimental sessions. **(C)** Trial structure with associated durations. After displaying CS, subjects were asked to choose which US they expected to follow. The US was then applied and rated in terms of its painfulness (for pain)/unpleasantness (for sound). EDA, electrodermal activity; CS, conditioned stimuli; US, unconditioned stimuli.

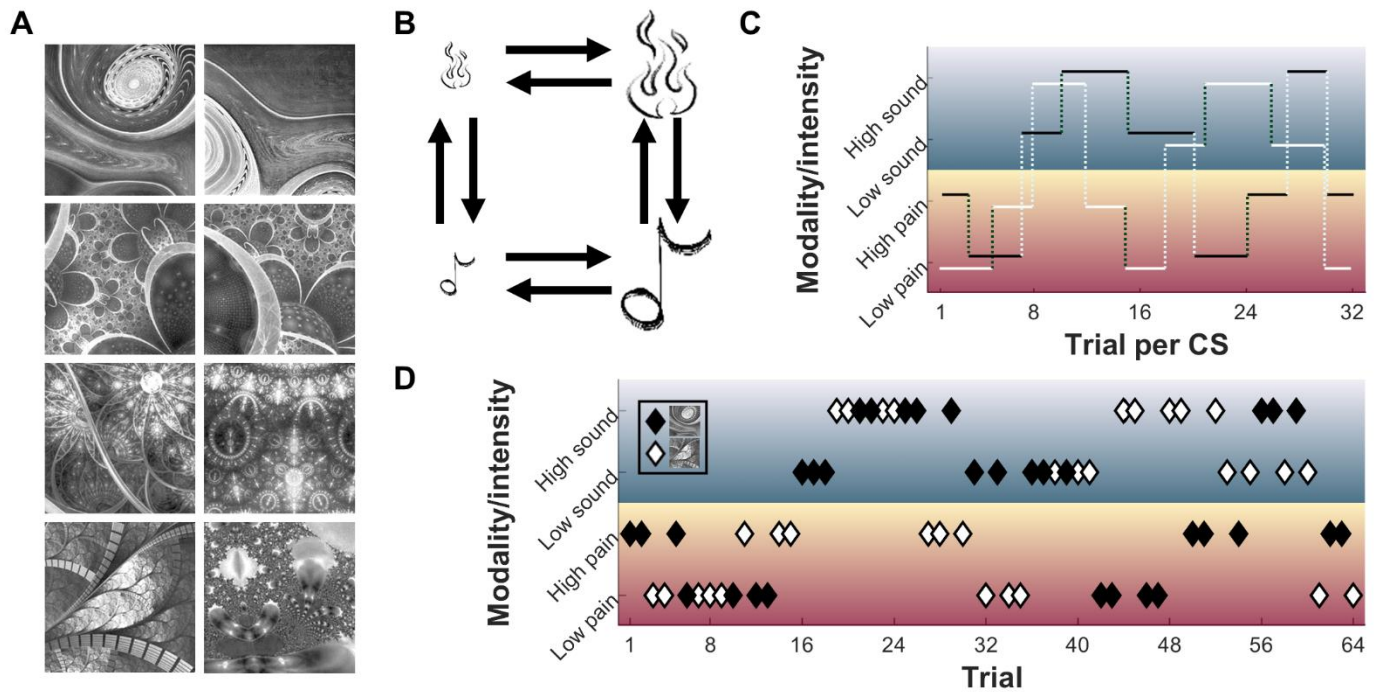


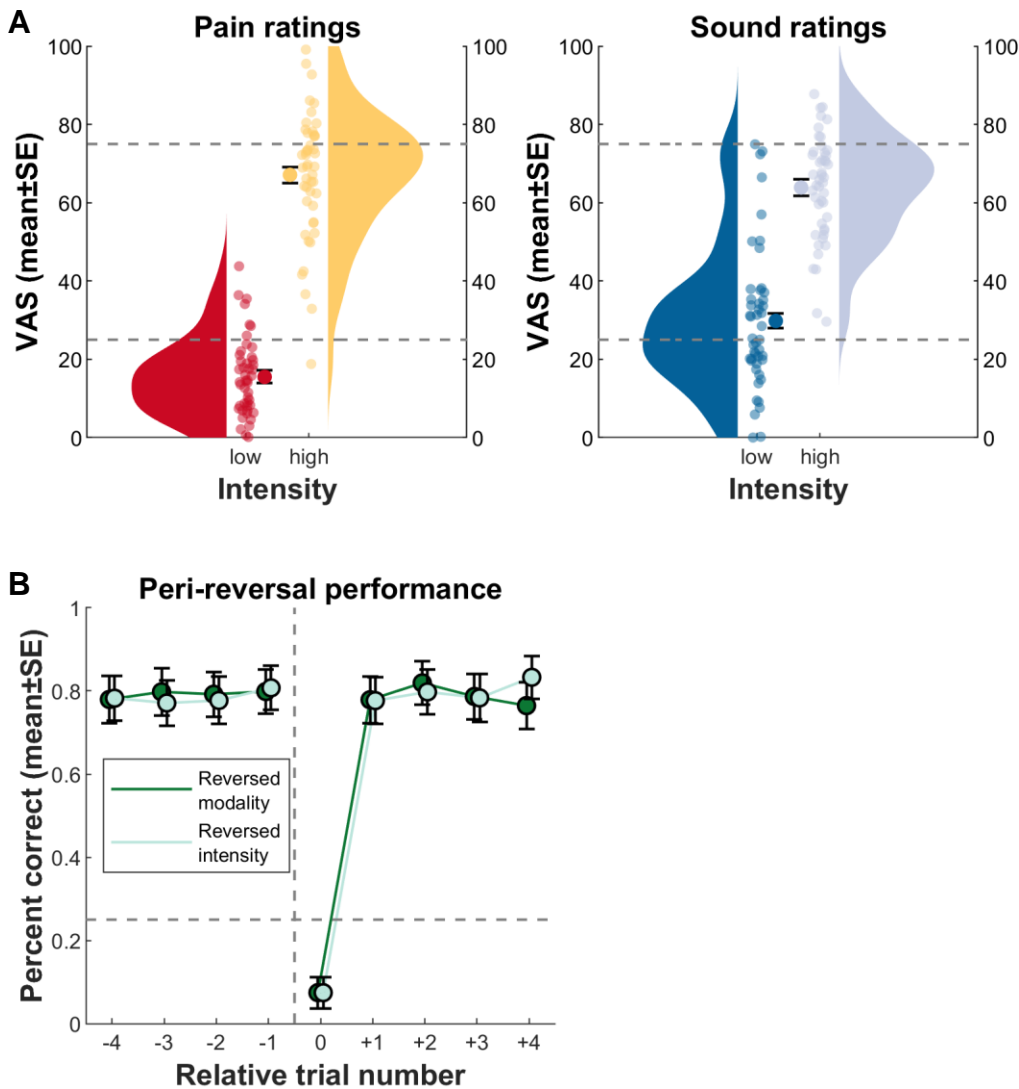
**Figure 2.** Learning protocol-related aspects of the experiment. **(A)** Set of conditioned stimuli; two were randomly selected for each subject (constraint: stimuli in row 2 could never both be selected due to high similarity). **(B)** Possible US associated with a CS at any particular trial (low pain, high pain, low sound, high sound). Arrows indicate possible reversals; notably, no combined intensity *and* modality (cross)reversals occurred. **(C)** Example for contingencies of CS1 (black solid line) and CS2 (white solid line) for their 32 trials per session each. Vertical dotted lines indicate reversals, with light dotted lines for modality reversals, dark dotted lines for intensity reversals. **(D)** Example for an actual trial sequence of 64 trials with interspersed CS1 (black diamonds) and CS2 (white diamonds), and their associated US (rows). CS, conditioned stimuli; US, unconditioned stimuli.

### Behavioral results: Calibrated stimulus intensities

Calibration yielded temperatures of  $44.4 \pm 1.2^\circ\text{C}$  for the less painful stimulus (25VAS) and  $46.8 \pm 1.2^\circ\text{C}$  for the more painful stimulus (75VAS). For sound, calibration yielded  $91.7 \pm 2.8\text{dBA}$  for the less loud sound (25VAS) and  $97.9 \pm 3.7\text{dBA}$  for the louder sound (75VAS). Distributions of calibrated stimulus intensities are displayed in Supporting Figure 2a.

### Behavioral results: Stimulus ratings

The first question concerning the behavioral data was whether ratings corresponded to the calibrated intensities (supposed to yield VAS of 25 and 75, respectively). Actual low pain ratings were at  $15.4 \pm 14.8\text{VAS}$ , high pain ratings at  $66.8 \pm 21.3\text{VAS}$ ; low sound ratings were at  $29.2 \pm 21.0\text{VAS}$ , high sound ratings at  $63.3 \pm 19.4\text{VAS}$  (Figure 3a; see Supporting Figure 2b for individual ratings per subject).



108

109

110 **Figure 3.** Behavioral results for pain ratings and performance. **(A)** Results for low and high unconditioned pain and sound stimuli; aggregate ratings of all pain and sound trials. Circles with error bars show the mean  $\pm$  standard errors over all subject means. Subject means are displayed as smaller circles. Violin plots aggregate over subject means. The grey dashed line is the “intended” rating as per calibration (VAS25 for low, VAS75 for high intensities). **(B)** Performance pre and post reversals, aggregated over all subjects. Circles indicate the performance during (peri)reversal trials, first averaged within and then between subjects (mean  $\pm$  standard errors). The dashed horizontal line marks chance level (25%, i.e. 1 of 4 options). The dashed vertical line indicates contingency reversal, with relative trial number 0 as the reversal trial. Note that no difference arose between trials preceding and following modality versus intensity reversals (also see Figure 2 for aspects concerning contingency reversals). Furthermore, the step increase in performance after trial number 0 indicates, on average, rapid learning of the new contingency.

119

## 120 Behavioral results: Learning performance

121 The next behavioral question was whether the subjects learned the CS/US contingencies. Figure 3b depicts mean performance in predicting the US currently associated with the CS, in relation to the reversals of the association.

122 Combining reversal types and comparing performance at the single trials prior reversal, at reversal, and after reversal,

123

124 we find pre-reversal performance to be above chance level ( $t[79] = 13.8, p \approx 0$ ), at reversal performance below chance  
125 ( $t[79] = -15.9, p \approx 0$ ), and post-reversal performance back above chance ( $t[79] = 19.5, p \approx 0$ ).

## 126 Skin conductance response results

127 The major question concerning SCR results were whether any differences between the US arose, and how the different  
128 PE types would be reflected in this psychophysiological measure of nonspecific characteristics or processes like arousal,  
129 salience, or surprise. SCR following sound has a faster onset than that following heat pain stimuli (Figure 4a; see  
130 Materials and Methods concerning the different response windows). The average amplitude of pain-related SCR was  
131 higher than the average of sound-related SCR, but this difference only showed a trend towards significance (main effect  
132 modality,  $t[4399] = -1.7228, p = 0.08499$ ). Instead, the difference is subsumed by a larger difference between low and  
133 high stimuli in the pain modality, as compared to that in the sound modality (modality\*intensity,  $t[4399] = -2.9739, p =$   
134  $0.0029567$ ). On average, higher stimuli lead to larger amplitude as well (main effect intensity,  $t[4399] = 8.2743, p = 1.7 \times$   
135  $10^{-16}$ ). Investigating this difference only in correctly predicted trials shows a similar effect on SCR (modality,  $t[2674] = -$   
136  $1.4379, p = 0.1506$ ; intensity,  $t[2674] = 8.0081, p = 2 \times 10^{-15}$ ; modality\*intensity,  $t[2674] = -4.6669, p = 3 \times 10^{-6}$ )  
137 (Supporting Figure 3, Supporting Table 1).

138 Further investigating SCR differences following PEs, we first distinguished SCR when subjects correctly predicted the US  
139 from trials when either an intensity PE or modality PE was made (Figure 4c). The following statistics include all trials –  
140 not just reversals – where an incorrect prediction was made. As shown in the first block (grey bars), over all US and  
141 controlling for modality and intensity, SCR following unsigned intensity PEs are larger than those following no PE  
142 (intPE>noPE,  $t[4397] = 4.336, p = 2 \times 10^{-05}$ ), while SCR following modality PEs are even larger (modPE>noPE,  $t[4397] =$   
143  $12.345, p = 2 \times 10^{-34}$ ; modPE>intPE,  $t[4397] = 6.398, p = 2 \times 10^{-10}$ ).

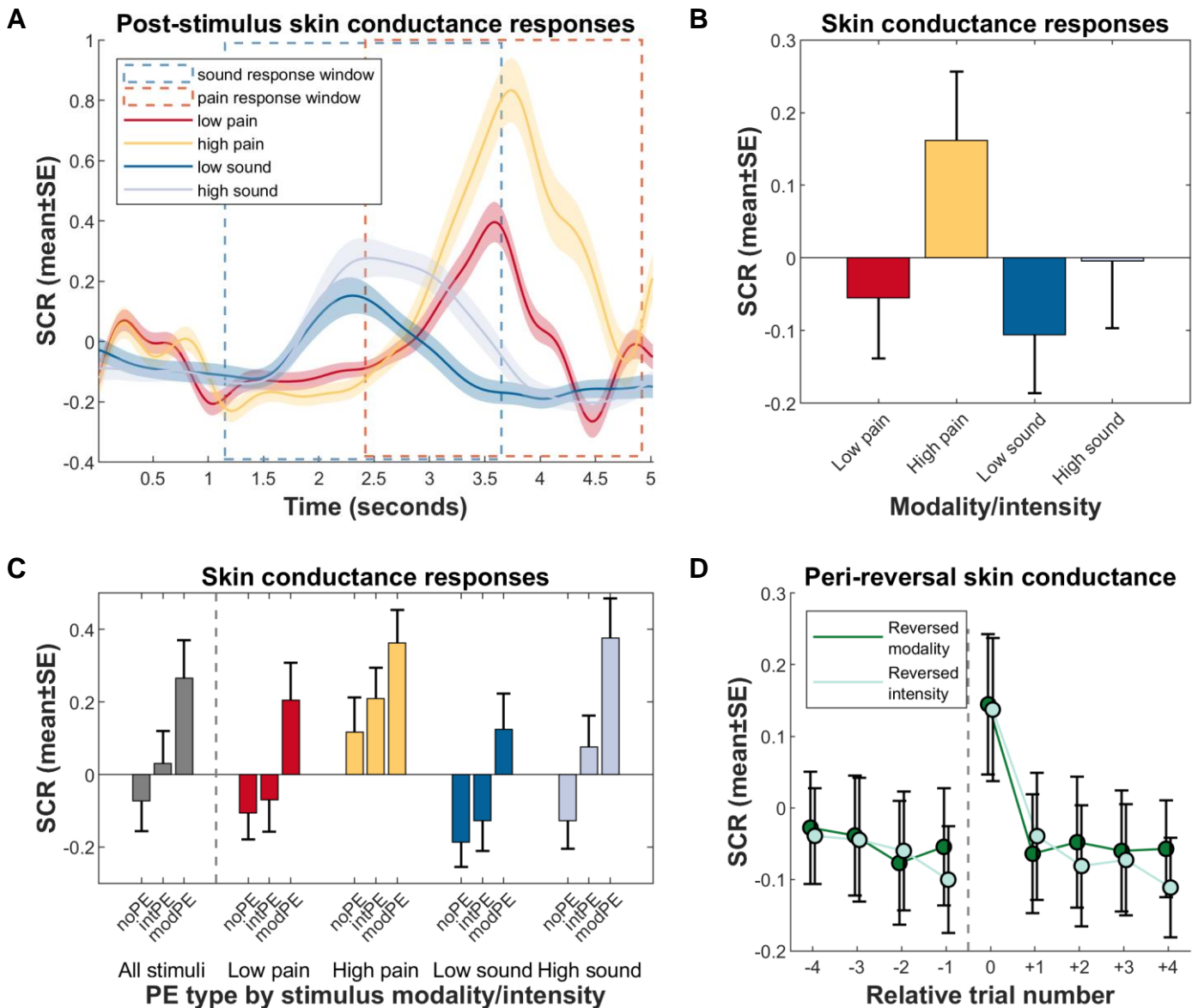
144 Notably, we performed an adjunct analysis on whether the direction of intensity PEs (i.e. signed intensity PEs) had an  
145 impact. We obtained mean SCR differences per subject between no PE and intensity PE trials for each modality and  
146 intensity separately, thereby accounting for higher intensity-related base SCRs; next, we contrasted these (now signed)  
147 PE-related differences between the low and high intensity. For pain, results indicate no effect (PE-related SCR difference  
148 for low pain mean $\pm$ SE 0.036 $\pm$ 0.052, for high pain 0.0922 $\pm$ 0.0622, paired t-test  $t[36] = -0.725, p = 0.4731$ ), while for  
149 sound, a more ambiguous yet non-significant result arose (PE-related SCR difference for low sound mean $\pm$ SE  
150 0.060 $\pm$ 0.054, for high sound 0.199 $\pm$ 0.054, paired t-test  $t[35] = -1.931, p = 0.0616$ ).

151 In four consequent analyses, we investigated differences in SCR following PEs in all US separately, meaning that all  
152 intensity PEs are now signed. Results indicate that the intPE>noPE effect of the global analysis is driven by this contrast  
153 in the high sound US (light blue bars,  $t[1119] = 4.732, p = 3 \times 10^{-6}$ ); it does not reach significance following any other US.



154 Conversely, modality PEs are followed by larger SCR in all US (all modPE>noPE  $p < 0.001$ ; smallest effect modPE>intPE  
155  $t[1090] = 2.045$ ,  $p = 0.041079$ ).

156 Figure 4d shows the average perireversal trial effect on SCR, over all US. It shows a large increase in SCR during both  
157 modality and intensity reversals; note that this analysis does not consider actual subject expectation, just the position  
158 related to the reversal trial. SCR is highest during the reversal trial, and rapidly reaches a lower plateau even one trial  
159 later. Comparing the pre-reversal trial to immediate post-reversal (trials -1 to +1), SCR is not significantly different if a  
160 modality reversal occurred ( $p = 0.54704$ ); this is also the case if an intensity reversal occurred ( $p = 0.071164$ ).



161

162

163

164

165

166

167

168

169

170

171

172

173

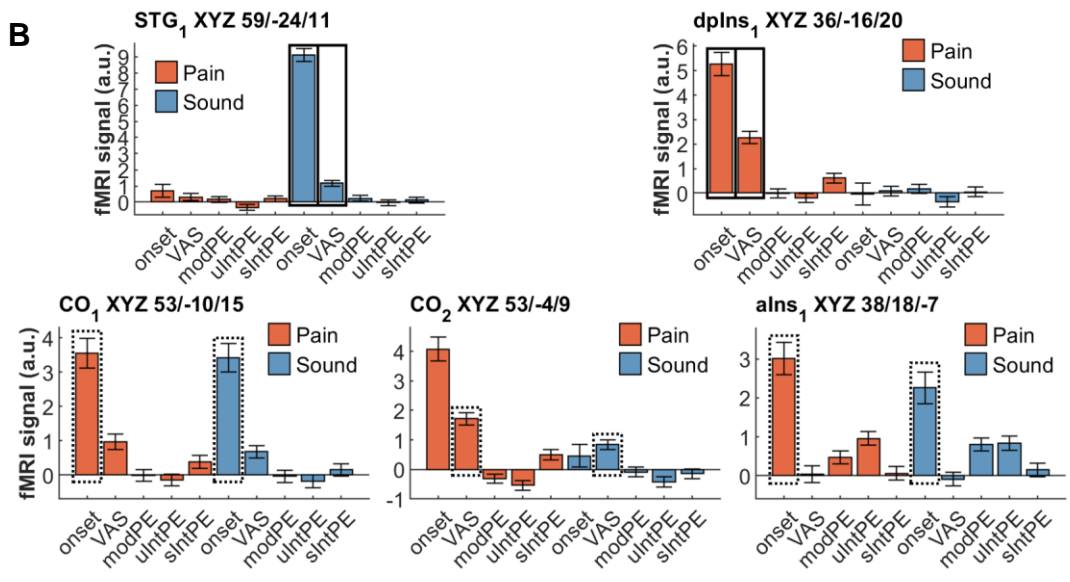
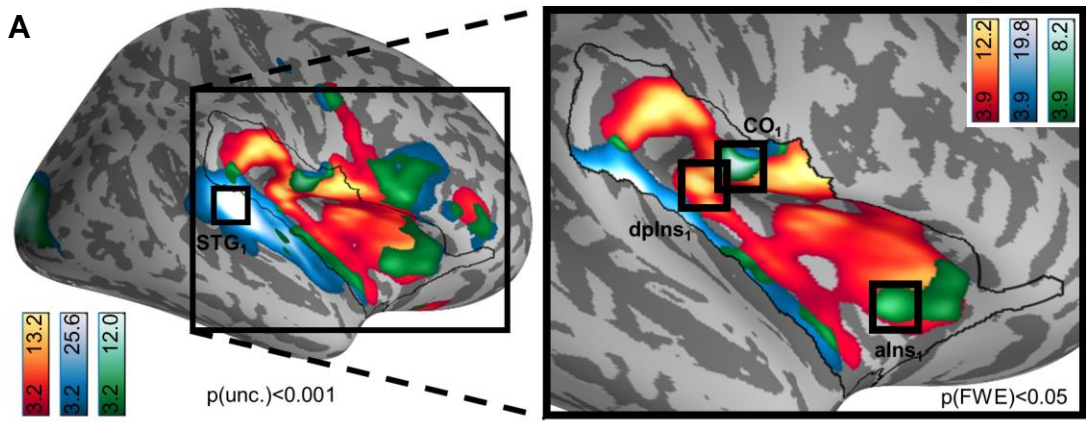
174

**Figure 4.** Results from skin conductance response measurements. All plots are based on log- and z-transformed data. **(A)** SCR in relation to unconditioned stimulus onsets, by US modality/intensity. Note the differences in latencies between the two modalities (pain in red/yellow has a later onset, sound in dark blue/light blue earlier), which determined the response windows used for mean SCR calculation in panel b. **(B)** Mean SCR by US, calculated within each modality's response window. On average, SCR is not significantly different between modalities; differences arise between intensities, and in the interaction of modality and intensity (see text for parameters). **(C)** Mean SCR by US and prediction error type. Over all modalities and intensities, differences arise between each PE type. Within specific modality/intensity combinations, differences between no PEs and intensity PEs only arise in the high sound condition. **(D)** Mean SCR in and around reversal trials. The dashed vertical line indicates contingency reversal, with relative trial number 0 as the reversal trial. SCR rises sharply after reversal, but quickly adapts post reversal to a stable level. SCR, skin conductance response; US, unconditioned stimulus; PE, prediction error; noPE, correct prediction; intPE, intensity prediction error; modPE, modality prediction error.

175 **Imaging results**

176 We first obtained an overview of modality-related effects (Figure 5a/b) and intensity-related effects (Figure 5b/c) of the  
 177 US. All locations are reported using Montreal Neurological Institute (MNI) coordinates (XYZ<sub>MNI</sub>). As expected, heat  
 178 stimulation was followed by larger activation in widespread insular and opercular areas, with the highest peak in the  
 179 dorsal posterior insula (XYZ<sub>MNI</sub> 35.5/-17.9/21.4, T = 12.2, p[corr.] = ~0). Notably, a conjunction of both heat and sound  
 180 main effects shows activation in the central operculum (XYZ<sub>MNI</sub> 53.0/-10.3/15.1, T = 8.3, p[corr.] = 8 x 10<sup>-13</sup>), dorsal  
 181 anterior insula (XYZ<sub>MNI</sub> 37.6/18.4/-7.0, T = 5.6, p[corr.] = 2 x 10<sup>-05</sup>), and several regions in between peaks for both  
 182 modalities.

183



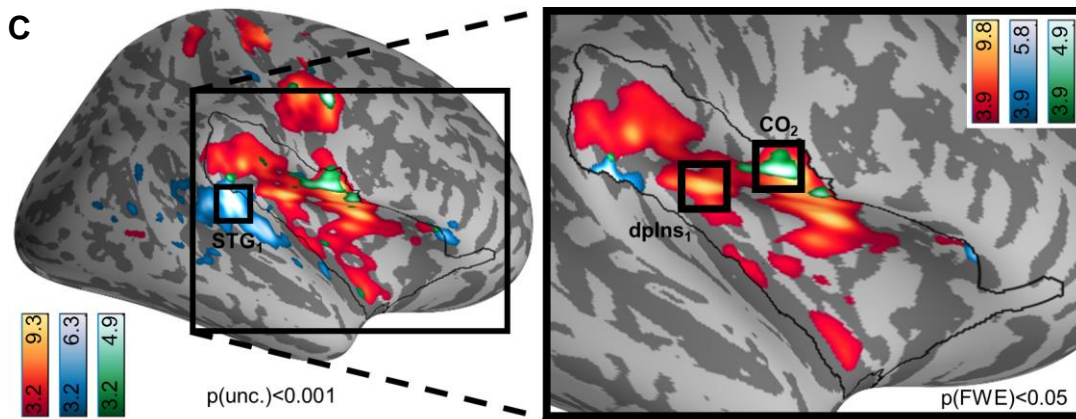


**Figure 5.** Brain activation following pain (red/yellow) and sound (blue), including overlaps as per conjunction analyses (green). Activations are overlaid on an average brain surface; for display purposes, activations in the whole brain lateral view are thresholded at  $p[\text{uncorr.}] < 0.001$ . The black line in the zoomed-in view delineates the region of interest and includes activations within the small volume FWE-corrected at  $p[\text{corr.}] < 0.05$ . Peaks are shown for small volume only; bar plots show beta weights of BOLD activation obtained from a general linear model (see Materials and Methods) from the respective peaks. See supporting information for peak positions in whole brain (Supporting Figure 4, Supporting Figure 6), and brain volume slices (Supporting Figure 5, Supporting Figure 7). **(A)** Differential and shared activation following painful heat stimulation and loud sound stimulation. Peak activation following heat is located in (peri)insular areas contralateral to stimulation, namely the dorsal posterior insula ( $\text{dpIns}_1$ ), and extending through the central and parietal opercula. Peak activation following sound is located in the superior temporal gyrus. Common activation (green) is located in the central operculum ( $\text{CO}_1$ ) and dorsal anterior insula ( $\text{aIns}_1$ ), among other regions. **(B)** fMRI signal (arbitrary units) for peaks detected in panel a (US onset effects) or c (parametric modulation by ratings). **(C)** Differential and shared correlations with pain ratings (for heat) and unpleasantness ratings (for sound). Activation correlated with pain ratings is focused on the dorsal posterior insula ( $\text{dpIns}_1$ ). Activation correlated with sound ratings is focused on the superior temporal gyrus. Conjunction activation peaks in central operculum ( $\text{CO}_2$ ) and precentral gyrus. fMRI signal regressor labels: VAS, visual analogue scale; PE, prediction error; modPE, modality PE; ulntPE, unsigned intensity PE; slntPE, signed intensity PE.

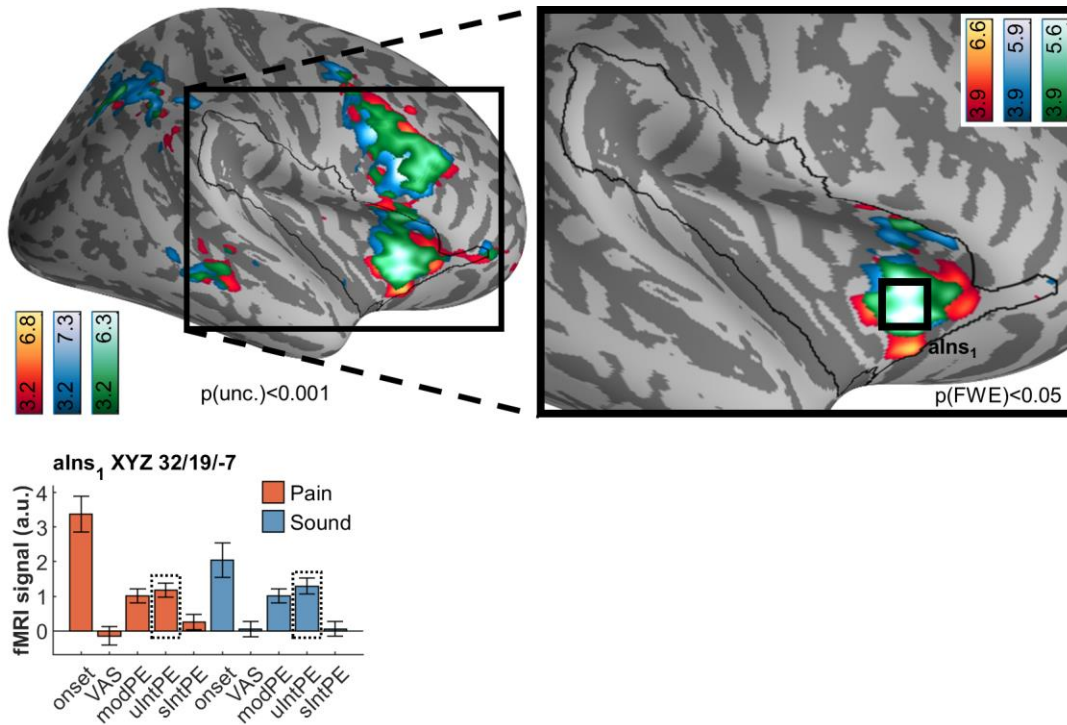
Next, we tested for fMRI responses correlated with stimulus perception, i.e. pain and sound VAS ratings (Figure 5b/c). For pain ratings, associations arose in the dorsal posterior insula ( $\text{XYZ}_{\text{MNI}} = 35.2, y = -17.4, z = 18.6, T = 7.2, p[\text{corr.}] = 1 \times 10^{-09}$ ). For sound ratings, we observed a peak directly adjacent to the small surface ( $\text{XYZ}_{\text{MNI}} 59.8, y = -33.9, z = 5.4, T = 4.8, p[\text{corr.}] = 0.016$ ). Common activation between pain and sound ratings peaked in the central operculum ( $\text{XYZ}_{\text{MNI}} 53.2, y = -2.7, z = 8.9, T = 4.8, p[\text{corr.}] = 0.001$ ). Of note, the central operculum peak ( $\text{CO}_2$  in Figure 5c) is located slightly anterior to that found for the modality conjunction ( $\text{CO}_1$  in Figure 5a) but shows barely any sound modality activation; conversely, peak  $\text{aIns}_1$  indicates that no intensity effects are encoded here. See supporting information for additional activations (Supporting Figure 4, Supporting Figure 6).

### Unsigned intensity prediction errors

Having ascertained strictly stimulus-related effects, our next analysis included an investigation of *unsigned* intensity PEs within and between either modality (Figure 6). The guiding question here was whether any differences and commonalities between the modalities would emerge. Since we used the actual expectation queried from subjects, “prediction error” here means that subjects explicitly expected one intensity but received the other. Consequently, the unsigned PE implies some extent of surprise.

217 In both modalities, widespread activation was observed. However, conjunction analyses revealed that the majority of  
 218 the observed activation actually overlapped between the modalities (green in Figure 6). The anterior insula constituted  
 219 the dominant cluster of this overlap, with symmetric bilateral peaks ( $XYZ_{MNI} = 34.6/23.5/-1.5$ ,  $T = 5.8$ ,  $p[\text{corr. wb.}] = 1 \times$   
 220  $10^{-04}$ ); whole brain-significant frontal (medial and lateral), temporal and parietal activation was also observed  
 221 (Supporting Figure 8).

222



223

224 **Figure 6.** Brain activation following unsigned intensity prediction errors in pain (red/yellow) and sound (blue), including overlaps as  
 225 per conjunction analyses (green). Peak activation following either modality is located in the anterior insula (alns<sub>1</sub>) and is subsumed in  
 226 the common activation. Activations are overlaid on an average brain surface; for display purposes, activations in the whole brain  
 227 lateral view are thresholded at  $p[\text{uncorr.}] < 0.001$ . The black line in the zoomed-in view delineates the region of interest and includes  
 228 activations within the small volume FWE-corrected at  $p[\text{corr.}] < 0.05$ . See supporting information for peak positions in whole brain  
 229 (Supporting Figure 8), and brain *volume* slices (Supporting Figure 9). fMRI signal regressor labels: VAS, visual analogue scale; PE,  
 230 prediction error; modPE, modality PE; ulntPE, unsigned intensity PE; slntPE, signed intensity PE.

231

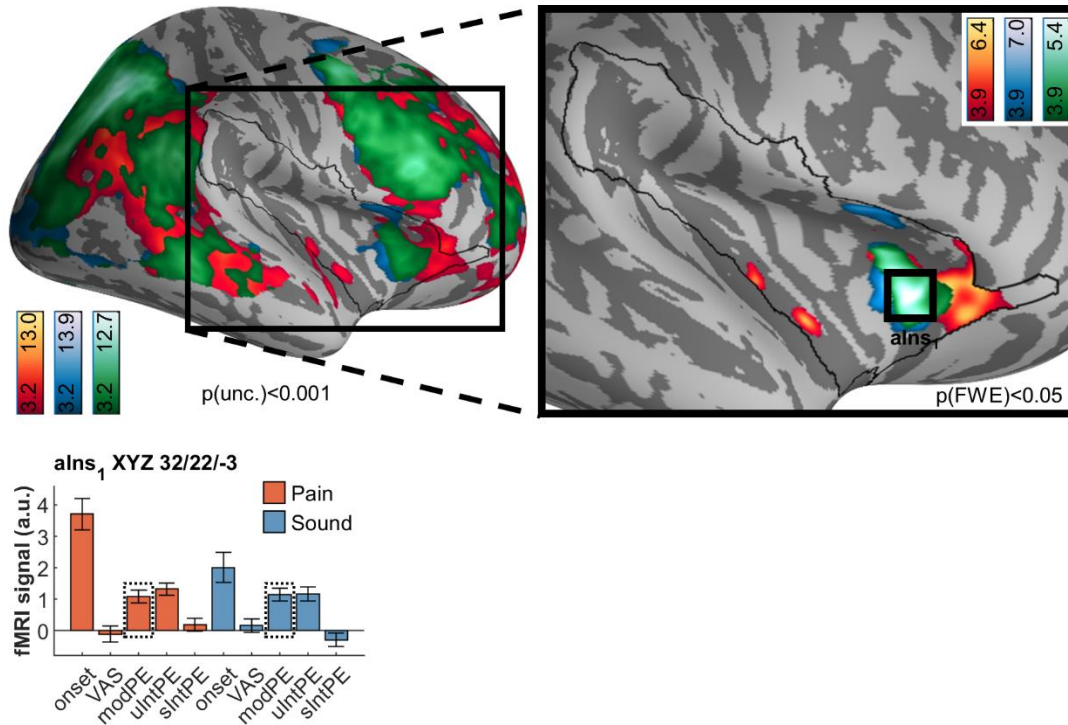
232 Two aspects were of particular interest to us considering unsigned intensity PE results: First, that brain activation related  
 233 to unsigned intensity PEs (Figure 6) was distinct from the intensity-related activation (Figure 5). Second, the fMRI signal  
 234 of the common activation in the anterior insula clearly indicated that modality PEs are likewise encoded in this area.

### 235 Modality prediction errors

236 Following these two observations, we proceeded to investigate the nature of the overlap between the two types of PE.  
 237 Like with unsigned intensity PEs, we observed widespread activation following each modality PE separately (Figure 7).

238 Likewise, all unimodal activation is subsumed in the conjunction analysis, which indicates a large dorsal anterior insula  
 239 cluster in our region of interest ( $XYZ_{MNI}$  32.3/22.4/-3.4,  $T = 5.4$ ,  $p[\text{corr.}] = 5 \times 10^{-05}$ ). Beyond this region, widespread  
 240 common activation is observed, for example, in the superior parietal lobule, precuneus, temporo-parietal junction,  
 241 middle frontal gyrus and frontal operculum, and medial orbital gyrus (Supporting Figure 10).

242



243

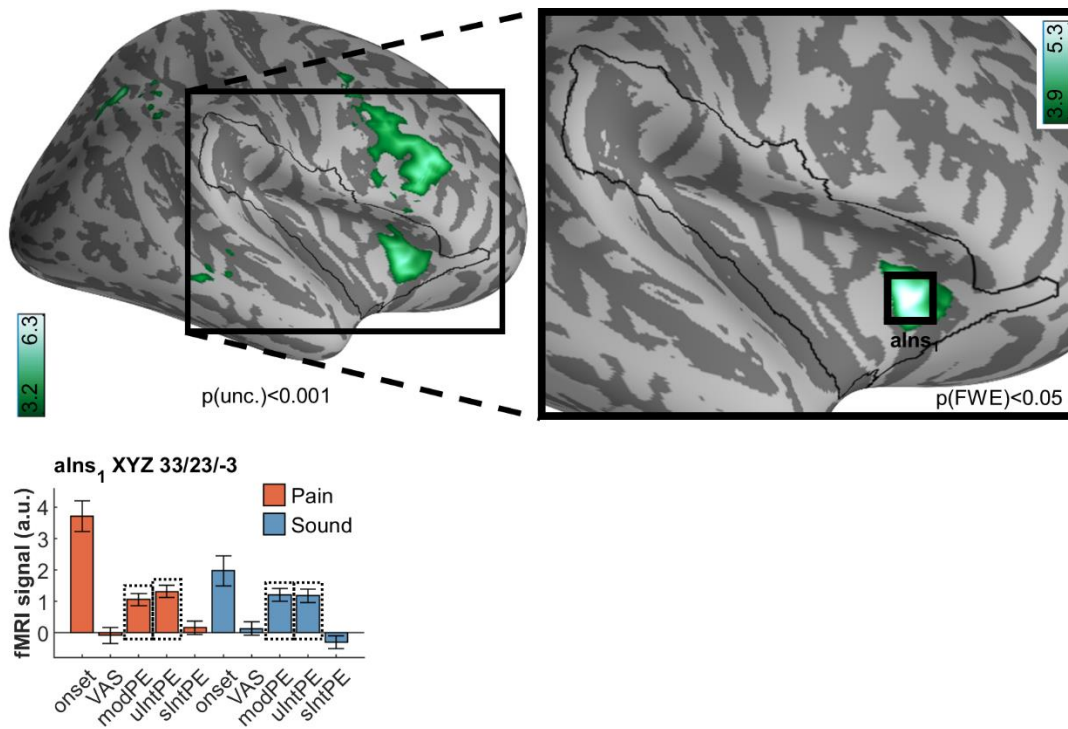
244 **Figure 7.** Brain activation following modality prediction errors in pain (red/yellow) and sound (blue) activation, including overlaps as  
 245 per conjunction analyses (green). As with unsigned intensity PEs, peak activation following modality PEs in either modality is located  
 246 in the anterior insula ( $alns_1$ ) and is largely subsumed in the common activation. Activations are overlaid on an average brain surface;  
 247 for display purposes, activations in the whole brain lateral view are thresholded at  $p[\text{uncorr.}] < 0.001$ . The black line in the zoomed-  
 248 in view delineates the region of interest and includes activations within the small volume FWE-corrected at  $p[\text{corr.}] < 0.05$ . Peaks are  
 249 shown for the small volume only. See supporting information for peak positions in whole brain (Supporting Figure 10), and brain  
 250 volume slices (Supporting Figure 11). fMRI signal regressor labels: VAS, visual analogue scale; PE, prediction error; modPE, modality  
 251 PE; ulntPE, unsigned intensity PE; slntPE, signed intensity PE.

252

### 253 [Overlap of unsigned prediction errors](#)

254 As a next step, we wanted to more formally assess the apparent overlap between both types of unsigned PEs. To do so,  
 255 we simply computed the conjunction between unsigned intensity and modality PE (Figure 8). This analysis corroborated  
 256 the anterior insula peak determined by separate analyses above. Furthermore, activation extended dorsally through the  
 257 middle frontal gyrus and also included medial prefrontal areas adjacent to the dorsal anterior cingulate cortex.

258



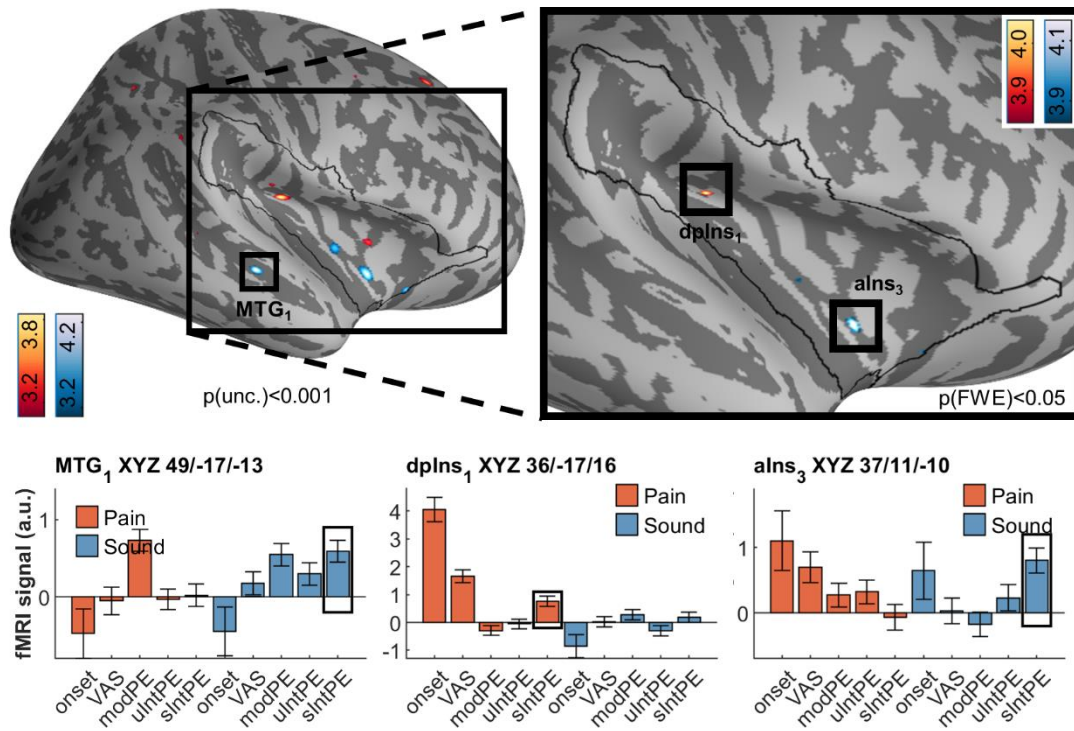
259

260 **Figure 8.** Common brain activation associated with unsigned intensity and modality prediction errors. The fMRI signal plot shows  
 261 that the peak in the anterior insula (aIns<sub>1</sub>) encodes PEs for every contrast included in the conjunction. Activations are overlaid on an  
 262 average brain surface; for display purposes, activations in the whole brain lateral view are thresholded at p[uncorr.] < 0.001. The  
 263 black line in the zoomed-in view delineates the region of interest and includes activations within the small volume FWE-corrected at  
 264 p[corr.] < 0.05. fMRI signal regressor labels: VAS, visual analogue scale; PE, prediction error; modPE, modality PE; ulntPE, unsigned  
 265 intensity PE; slntPE, signed intensity PE.  
 266

## 267 Signed intensity prediction errors

268 After ascertaining the effects for *unsigned* PEs for both intensity and modality, the final question for our fMRI data  
 269 referred to differences and commonalities following *signed* intensity PEs, i.e. correlations of brain activation with higher-  
 270 than-expected intensity (Figure 9). For pain, we observed an activation in the dorsal posterior insula (XYZ<sub>MNI</sub> 36.4/-  
 271 17.3/15.8, T=4.0, p[corr.]=0.023). The dorsal posterior insula is an area considered of fundamental importance for the  
 272 processing of pain intensity [24,28,31]. For sound itself, the peak activation was observed outside the region of interest,  
 273 in the middle temporal gyrus (XYZ<sub>MNI</sub> 49.4/-16.6/-13.4, T=4.1, p[uncorr.]=2 x 10<sup>-05</sup>) (see Figure 6). Within the region of  
 274 interest, sound-related activation was found in the anterior insula (XYZ<sub>MNI</sub> 36.7/11.0/-10.2, T=4.2, p[corr.]=0.015).  
 275 Notably, these are adjacent to the unsigned PE activations (Figure 6 through Figure 8). All signed intensity PE peaks, both  
 276 for pain and sound, show no significant representation of a signed PE in the other modality (see opposite slntPE fMRI  
 277 signals in Figure 9). Consequently, a conjunction analyses revealed no overlap.

278



279

280

281

282

283

284

285

286

287

288

**Figure 9.** Brain activation associated with by signed intensity prediction errors in pain (red/yellow) and sound (blue), including overlaps as per conjunction analyses (green). Contrary to ulntPEs, circumscribed activation was detected for pain slntPEs without any overlap with sound slntPEs. Peak activation is located in the dorsal posterior insula (dplns<sub>1</sub>). For sound, several clusters in the anterior insula (e.g. alns<sub>3</sub>) were found, as well as middle temporal gyrus (MTG<sub>1</sub>). Activations are overlaid on an average brain surface; for display purposes, activations in the whole brain lateral view are thresholded at  $p(\text{uncorr.}) < 0.001$ . The black line in the zoomed-in view delineates the region of interest and includes activations within the small volume FWE-corrected at  $p(\text{corr.}) < 0.05$ . fMRI signal regressor labels: VAS, visual analogue scale; PE, prediction error; modPE, modality PE; ulntPE, unsigned intensity PE; slntPE, signed intensity PE.

289

290

291

292

293

294

295

296

297

298

In summary, the unsigned intensity PE for pain and sound, as well as their modality PE, strongly overlap in the anterior insula (Figure 6), whereas signed intensity PE are accompanied by pain-dedicated activation in the dorsal posterior insula (Figure 9).

## Discussion

294

295

296

297

298

Using a Pavlovian learning paradigm with frequent reversals within and across aversive modalities in combination with SCR recordings and high resolution fMRI, we were able to investigate signed and unsigned representations of PE in the human brain. The data showed an unsigned representation of intensity PE in the anterior insula indistinguishable for pain and aversive sounds, supporting a role of the anterior insula in coding unspecific arousal or salience. In addition, the same part of the anterior insula also strongly activated for PE concerning stimulus modality. Most importantly, we



299 could identify a circumscribed part of the dorsal posterior insula representing a signed PE for pain only, collocated with  
300 areas processing pain intensity per se.

301 The parallel assessment of SCR, behavioral ratings for both expectation and outcome, as well as fMRI recordings allowed  
302 us to investigate PEs in a multimodal fashion. Previous studies investigated PEs using cue-based pain paradigms  
303 [12,19,21,32]. In these paradigms, a cue predicts a pain intensity with a certain probability. However, the probability also  
304 determines the number of trials in which a PE occurs. This can lead to unbalanced designs in which certain PEs occur  
305 much more frequently than others. In addition, the fixed association of a specific cue with an outcome risks that specific  
306 features of the cue influence PE processing. Adopting a Pavlovian transreinforcer paradigm ameliorates these  
307 shortcomings, and requires frequent relearning of contingencies and thus generates frequent PEs [22,23]. By defining a  
308 Markovian transition structure, we also controlled the nature of reversals; we confined our experiment to within-  
309 intensity/between-modality, and between-intensity/within-modality reversals. Finally, introducing two CS in our task  
310 increased task difficulty.

311 We explicitly included expectation ratings, which allowed us to use the difference between the US and its expectation as  
312 a rating-derived PE [22]. Compared to model-derived PEs, this can account for within-subject differences in learning and  
313 can also capture PEs in erratic behaviors difficult to model in formal reinforcement learning models.

314 Although we aimed to perfectly match salience between stimulus modalities, high intensity painful stimuli lead to higher  
315 SCR activation compared to low pain or either sound intensity (Figure 4), even though average SCR amplitudes between  
316 modalities were not statistically different. Technically, this is related to the fact that we were not able to increase sound  
317 pressure levels above a certain level [33] to avoid harm for the volunteers. However, the fMRI signal changes in the  
318 anterior insula for unsigned intensity PEs were similar for pain and sound, suggesting that the residual differences in SCR  
319 did not affect our results (Figure 6, Figure 7, Figure 8). In addition, previous accounts [34] have indicated that higher  
320 salience enhances memory performance. We tested this and observe no such effect: learning performance did not  
321 substantially differ between any of the US groups (Supporting Figure 14).

322 We have replicated findings concerning pain-related activation in the dorsal posterior insula/parietal operculum and  
323 sound-related activation in the superior temporal gyrus [24]. Previously, these areas showed a clear effect of pain and  
324 sound stimulation, respectively, but a crucial intensity-related increase in activation that is shallower or absent in non-  
325 noxious intensities. In contrast to the previous study, we see a stronger correlation of the BOLD response to sound  
326 ratings, possibly owing to the higher intensities employed here.

327 Also in agreement with previous studies, we observed an unsigned intensity PE for pain in the anterior insula [12,19,21].  
328 The novel contribution is the fact that stimuli in different modalities (i.e. pain and aversive sounds) [24] lead to the same  
329 activations in the anterior insula, with similar magnitudes. To our surprise, strong activation in the anterior insula was

330 also observed for modality PEs (expect pain and receive sound, and vice versa). fMRI signals for unsigned intensity PEs  
331 and modality PEs were very similar in magnitude. This disconfirms our hypothesis that at the level of the insula, modality  
332 PE carries less difference in salience between the expected and the real outcome, as compared to an unsigned intensity  
333 PE. Rather, it seems that surprise from unexpected sensory modalities is as much a source of anterior insula activation as  
334 from unexpected intensities. Our findings suggest that modality and unsigned intensity PEs are largely modality-neutral,  
335 and support findings that the anterior insula is richly interconnected part of the salience and attentional network  
336 involved in decision-making, error recognition and generally the guidance of flexible behavior [35–39]. Indeed, the  
337 large-scale activation following modality PEs and unsigned intensity PEs themselves does not correspond to any single  
338 network description, but seems to involve all of the above; possibly, different dynamics are at play over the course of  
339 the stimulation, which do not allow for the disentangling of single networks. In fact, recent meta-analytic evidence of  
340 resting-state functional connectivity points to the existence of a pain-related network centered on the anterior insula  
341 [40]. The activation associated with both pain-related (posterior insula) activation, and that associated with PE-related  
342 (anterior insula) activation correspond well with connectivity gradients observed along the posterior-anterior axis [41–  
343 43].

344 It is known that SCR predominantly shows arousal and similar effects, but is relatively insensitive concerning valence  
345 [25–27,44,45]. Here, SCR following unsigned or signed intensity PEs was little different from SCR following no PEs, while  
346 SCR following modality PEs was much higher. This might indicate that modality PEs provide a highly salient a teaching  
347 signal even in the absence of intensity differences (Supporting Figure 3).

348 A signed representation of an intensity PE for pain is a crucial teaching signal in reinforcement learning, as it is important  
349 to dissociate a low threat from a high threat stimulus. Such a representation for pain could plausibly be located in an  
350 area adjacent the anterior insula part representing unsigned intensity PEs and modality PEs. Alternatively, this  
351 representation could be located closer to representations of pain intensity: Coding of signed intensity PEs within areas  
352 coding for stimulus intensity per se was observed using a similar Pavlovian transreinforcer paradigm in the olfactory  
353 domain [23]. Indeed, our data show that a signed intensity PE for pain is represented in a part of the dorsal posterior  
354 insula [24,28]. Interestingly, we also identified a similar representation of a signed intensity PE for aversive sounds in or  
355 adjacent to primary auditory cortices [46,47], namely the middle temporal gyrus and temporal operculum. It also seems  
356 indicative of the more general involvement of the insula in pain perception [48] that the signed intensity PE in pain has  
357 little to none sound-related activation at all, whereas the signed intensity PE in sound includes some pain intensity-  
358 related activation.

359 At most, the clear spatial dissociation of intensity PEs for pain and sounds furthermore indicates a specificity of the  
360 signal; at least, it stands in marked contrast with the large overlap of activation for unsigned intensity and modality PEs  
361 in the anterior insula. Powerful learning models can utilize both a signed PE to update their predictions and an unsigned

PE to update their learning rate [10,17,18]. Our results provide a neuronal basis for these models as we were able to reveal the simultaneous representation of both a signed and unsigned PE signal in spatially distinct regions of the insula.

Due to the task-inherent structure, signed pain intensity PEs can be correlated with actual pain intensity [49]. This collinearity can be remedied by orthogonalizing regressors in the general linear model used for fMRI analysis. However, this arbitrarily assigns the shared variance to either of the two correlated regressors, depending on the order of the serial orthogonalization [50]. Therefore, we refrained from any orthogonalization in our analysis and thus only reveal areas that show unique variance tied to the regressors, including the signed intensity PEs for pain.

In conclusion, our data provides clear evidence of anterior insula-centered, modality-independent *unsigned* PEs, not only concerning mismatched stimulus intensities across modalities, but also across sensory modalities themselves. Equally important, *signed* intensity PEs were associated with activation in or adjacent to sensory areas highly dedicated to unimodal processing. Neuronal data from both sources are the basis for reinforcement learning and further enhance our understanding of the functional synergies within the insula. Importantly, pathological learning mechanisms [1,9] and abnormalities in anterior insula-related function have been reported in chronic pain [40,51]. Our data therefore offers the possibility that a misrepresentation of PEs constitutes a potential mechanism in pain persistence.

## Materials and Methods

The protocol conformed to the standards laid out by the World Medical Association in the Declaration of Helsinki and was approved by the local Ethics Committee (Ethikkommission der Ärztekammer Hamburg, vote PV4745). Participants gave written informed consent prior to participation and were aware of all aspects of the protocol except the randomized time point of reversal trials.

### Subjects

Forty-nine healthy volunteers (Sex 27f:22m, Age 26.2±4.5) were recruited through online advertisements ([www.stellenwerk.de](http://www.stellenwerk.de)) and word of mouth. They were screened concerning study- and MR-specific exclusion criteria as follows:

- Age younger than 18, older than 40
- Insufficient visual acuity (correction with contact lenses only)
- Conditions disqualifying for MR-scanners (e.g. claustrophobia, wearing a pacemaker)
- Ongoing participation in pharmacological studies, or regular medication intake (e.g. analgesics)
- Analgesics use 24h prior to the experiment
- Pregnancy or breastfeeding

- 392     ▪ Chronic pain condition
- 393     ▪ Manifest depression (as per Beck Depression Inventory II, cutoff 14 [52])
- 394     ▪ Somatic symptom disorder (as per Patient Health Questionnaire, cutoff 10 [53])
- 395     ▪ Other neurological, psychiatric or dermatological conditions
- 396     ▪ Inner ear conditions
- 397     ▪ Head circumference >60 cm (due to MR scanner coil/headphone constraints)

398 Eligible subjects were scheduled for a single lab visit. Experiments were conducted from October 2019 through March  
399 2020. Statistics characterizing the sample are listed in Supporting Table 2.

## 400 [Overview of the experiment](#)

401 The sequence of measurements and timings of the protocol are displayed in Figure 1, while aspect pertaining to CS  
402 characteristics as well as contingencies are displayed in Figure 2. The experiment lasted about 2.5 h. The experiment  
403 followed a full cross-over design, with every subject participating in all conditions. Subjects learned associations of  
404 conditioned stimuli (CS) and unconditioned stimuli (US; painful heat or loud sound). These associations eventually  
405 changed in an unforeseeable manner and then had to be relearned. The experiment was run in a single visit, but split  
406 into two sessions to reduce subject fatigue and carry-over effects. Prior to the experimental sessions, subjects were  
407 calibrated according to their pain and sound sensitivity. At the start and the end of the experiment, subjects filled out  
408 psychological questionnaires outside the scanner. Electrodermal activity was measured throughout the experimental  
409 sessions.

## 410 [Unconditioned stimuli](#)

411 Heat stimuli were delivered using a CHEPS thermode (Medoc, Ramat-Yishai, Israel) attached to the volar forearm. Basic  
412 stimulus parameters included a 32°C baseline temperature and 10°C/s rise and fall rates. Sound stimuli were delivered  
413 using MR-compatible headphones (MR confon, Magdeburg, Germany). A pure sound (frequency 1000 Hz, sampling rate  
414 22050 Hz) was generated during runtime using MATLAB.

## 415 [Calibration of unconditioned stimulus intensities](#)

416 Prior to the experiment proper, subjects underwent US calibration to determine two intensities at VAS 25 and VAS 75  
417 for both modalities (heat and sound). During the experiment, only these four stimuli were used. All stimuli lasted 3s at  
418 plateau, except for four 10s long, low-intensity preexposure stimuli used for familiarization and pre-heating of the skin.

419 Heat and sound stimuli were presented and rated in an analogous fashion. Like in a previous study comparing neuronal  
420 responses to the two modalities [24], we used the descriptor “painfulness” for heat, while we used the descriptor  
421 “unpleasantness” for sound. After calibration, all stimuli were above the respective pain and unpleasantness thresholds  
422 and were therefore displayed on simple 0 to 100 visual analogue scales (VAS) for both modalities.

423 For heat, anchors were displayed for “minimal pain” (0) and “unbearable pain” (100). Pain was defined as the presence  
424 of sensations other than pure heat intensity, such as stinging or burning [54].

425 For sound, subjects were instructed to rate between anchors labelled “minimally unpleasant” (0) and “extremely  
426 unpleasant” (100). Unpleasantness was defined as a bothersome quality of the sound emerging at a certain loudness.

427 During the calibration procedure performed in the running MR scanner, two stimulus intensities each were obtained for  
428 the heat and sound modality (low/high pain and low/high noise). Heat stimuli ranged from 43 to 49°C, sound stimuli  
429 ranged from 89.1 through 103.0 dBA. Calibration was constrained such that subjects had to reach a certain

- 430     ▪ minimum physical intensity (43°C for heat, 20% system volume for sound, n=1 received 10%)
- 431     ▪ minimum physical difference between the VAS 25 and 75 stimuli (1.5°C for heat, 15% system volume for sound;  
432         n=1 received 1°C, n=8 received 10%)

433 If either condition was not met, physical intensities were automatically adjusted to the minimum (e.g., if subject  
434 reported VAS 25 for 41°C, temperature was raised to 43°C). Furthermore, to ensure discriminability within stimulus  
435 modalities, subjects had the calibrated US played back to them and were explicitly asked three questions, namely that  
436 both intensities of the respective modality

- 437     ▪ were painful (for heat) or unpleasant (for sound)
- 438     ▪ were perspective tolerable throughout repeated trials in two sessions
- 439     ▪ were easily discriminable.

440 If either question was answered in the negative, the calibrated intensities were adjusted, but never below the minimum  
441 requirements listed above.

## 442 [Learning protocol](#)

443 Learning the CS-US associations was designed as a Pavlovian transreinforcer reversal learning task [22,23]. Two CS would  
444 independently predict one of four US, namely two intensities of painful heat and two intensities of unpleasant sound.  
445 Subjects were presented with one of the two CS (Figure 2c and d) and then asked to choose which of the four US they  
446 believed to be preceded by it (symbols in Figure 2b). After making their choice, they would actually be exposed to one of  
447 the four US (see Figure 1c for trial structure). If they were correct, no further learning was required; if not, they would  
448 have the opportunity to learn the correct association for the next occurrence of the CS. They would then rate their pain  
449 or unpleasantness on a 0-100 visual analogue scale (VAS), as during US calibration. Both CS signified an independent  
450 sequence of associations with the US. Both CS were randomly drawn for each subject from a library of eight fractal  
451 pictures (Figure 2a). Which of the two CS was presented in each trial was fully randomized, as were the US for the  
452 respective initial associations, and the display order of the US prediction rating.

Crucially, after a number of trials with deterministic CS-US association, the association underwent an unannounced reversal either in terms of intensity (previously low US intensity would now be high, or vice versa), or modality (previous pain US would now be a sound US, or vice versa) (Figure 2c and d). The number of trials that an association was upheld was randomly determined from [3, 3, 4, 5] (i.e. 3.75 trials on average). After each reversal, subjects therefore made an error in predicting the following US, and subsequently had to learn the new association. As reversals on both dimensions were precluded, each session included eight reversals per CS to cover all possible reversals. Task performance was assessed by the percentage of correct predictions.

### Psychological questionnaires

Prior to and immediately after the experiment, subjects filled out several questionnaires assessing state and trait psychological constructs. These are listed in Supporting Table 2 alongside statistics characterizing the sample.

### Psychophysiological recordings

Electrodermal activity was measured with MRI-compatible electrodes on the side of the left hand opposite the thumb. Electrodes were connected to Lead108 carbon leads (BIOPAC Systems, Goleta, CA, USA). The signal was amplified with an MP150 analog amplifier (also BIOPAC Systems). It was sampled at 1000 Hz using a CED 1401 analog-digital converter (Cambridge Electronic Design, Cambridge, UK) and downsampled to 100 Hz for analysis.

Analysis was performed using the Ledalab toolbox for MATLAB [55]. Single subject data were screened for artifacts which were removed if possible by using built-in artifact correction algorithms. Of 47 subjects, 1 was excluded due to equipment malfunction, 9 due to skin conductance non-responsiveness. From the remaining 37 subjects, a total of 101 of 6016 segments (1.7%) were excluded due to unsalvageable artefacts. Using a deconvolution procedure, we computed the driver of phasic skin conductance (skin conductance responses, SCR). Stimulus phase response windows were offset between the two stimulus modalities [24] – we attribute an earlier onset following acoustic stimulation to reduced latency from the delivery system and neuronal transmission. To determine response windows, we obtained the times for average peaks of the respective modality, and selected the data range  $\pm 1.25$  s: For pain, response windows were set between 2.42 s and 4.92 s, and between 1.15 s and 3.65 s for sound. SCR segments were log- and z-transformed within subjects to reduce the impact of intra- and interindividual outliers [25]. Subsequently, segments were averaged within subjects for several conditions corresponding to the behavioral performance of subjects (e.g. intensity PE following low painful stimulation, or high painful stimulation). SCR was used because it is an objective measure of general sympathetic activity, and therefore a measure of arousal, stimulus salience and several associated psychological processes [25,26,45,56,57]. It is routinely used in assessing painful [12,24,58] as well as acoustic stimulation [59].

## 482 fMRI acquisition and preprocessing

483 Functional and anatomical imaging was performed using a PRISMA 3T MR Scanner (Siemens, Erlangen, Germany) with a  
484 20-channel head coil. An fMRI sequence of 56 transversal slices of 1.5 mm thickness was acquired using T2\*-weighted  
485 gradient echo-planar imaging (EPI; 2001 ms TR, 30 ms TE, 75° flip angle, 1.5x1.5x1.5 mm voxel size, 1 mm gap,  
486 225x225x84 mm field of view, simultaneous multislice imaging with a multiband factor of 2, and an acceleration factor  
487 of 2 with generalized autocalibrating partially parallel acquisitions reconstruction). Additionally, a T1-weighted MPRAGE  
488 anatomical image was obtained for the entire head (voxel size 1x1x1 mm, 240 slices).

489 For each subject, fMRI volumes were realigned to the mean image in a two-pass procedure, and non-linearly co-  
490 registered to the anatomical image using the CAT12 toolbox for SPM (Christian Gaser & Robert Dahnke,  
491 <http://www.neuro.uni-jena.de/cat/>). In short, this novel non-linear coregistration segments both the mean EPI and the  
492 T1 weighted image and performs a nonlinear spatial normalization of the segmented tissue classes from the mean EPI  
493 using the segmented tissue classes from the T1 scan as a template. Finally, individual brain surfaces were generated,  
494 using CAT12.

## 495 General statistical approach

496 Unless otherwise noted, analyses except the fMRI analyses were performed using linear mixed models with random  
497 intercept using trial-by-trial parameters. In the case of mixed (within/between) descriptive statistics, standard errors  
498 were calculated using the Cousineau-Morey approach [60]. The significance level for analyses of behavioral and  
499 psychophysiological data was set to  $p = 0.05$ .

## 500 Analysis of imaging data

501 Subject-level analyses were performed on the 3D (volume) data in native space without smoothing, as required for  
502 surface mapping. We computed a general linear model with a canonical response function to identify brain structures  
503 involved in the processing of each stimulus modality, and corresponding to various predictions and PEs inherent in the  
504 protocol. Realignment (motion) parameters were included as nuisance variables, to further mitigate motion-related  
505 artifacts.

506 A general linear model was set up with one regressor for stimulus main effects in each modality (heat or sound), and a  
507 parametric modulator each for pain or unpleasantness (using behavioral ratings). An additional three parametric  
508 modulators for each modality were entered for modality PEs and intensity PEs: Modality PEs were entered unsigned due  
509 to their non-parametric nature, whereas intensity PEs were entered both unsigned (absolute) and signed. All parametric  
510 modulators were z-scored within subjects and sessions. In either model, global or sequential orthogonalization between  
511 regressors were turned off to preserve only the unique (non-shared) variance components [23,50]. This approach allows  
512 for the interpretation of consecutively entered parametric modulators even if correlations to previous regressors exist.

513 We opted for surface-based analyses of fMRI data to enhance discrimination between modalities processed in adjacent  
514 brain regions [24]; for an example of pseudo-overlap detected across the sylvian fissure, see Supporting Figure 5 (row 3),  
515 particularly in slices -28 through -16. Results from subject-level analyses were mapped to brain surfaces obtained via the  
516 CAT12 segmentation procedure. The mapped subject-level results were then resampled to correspond to cortical  
517 surface templates, and smoothed with a 6 mm full width-half maximum 2D kernel. Group-level within-subjects analyses  
518 of variance were performed including the mapped contrasts. The original, unmapped contrasts were used for volume-  
519 based group-level analyses to assess subcortical activation. Volume results were then warped using DARTEL  
520 normalization and smoothed with a 6 mm full width-half maximum 3D kernel. Volume-based results are provided in the  
521 supporting information and referenced where relevant.

522 Contrasts employed for any of the analyses were either performed against low-level baseline (e.g. Pain>0), as a  
523 conjunction of a differential modality contrast and one against low-level baseline (e.g. Pain>Sound  $\wedge$  Pain>0), or as a  
524 conjunction of both modalities (e.g. Pain  $\wedge$  Sound).

### 525 [Regions of interest and statistical correction of imaging results](#)

526 As laid out above and because pain is the modality of interest in this study, we focused the analyses on the contralateral  
527 (right) periinsular cortices as regions of interest used for small volume correction of significance level [12,19,24]. The  
528 region of interest included the entire insular cortex (dorsal hypergranular, dorsal granular, dorsal dysgranular, dorsal  
529 agranular ventral dysgranular/granular, ventral agranular), as well as dorsally adjacent areas of the parietal operculum  
530 (A40rv), central operculum (A1/2/3II, A4tI) and frontal operculum (A44op, A12/47I). It was created using the Human  
531 Brainnetome Atlas [61]. Results were considered after correction for family-wise error rate of  $p < 0.05$  within the region  
532 of interest (denoted  $p[\text{corr.}]$ ), or after correction for whole brain/all vertices (denoted  $p[\text{corr. wb.}]$ ), unless otherwise  
533 noted.

534



## 535 Acknowledgements

536 This work was supported by ERC-AdG-883892-PainPersist and DFG SFB 289 Project A02 (Project-ID 422744262–TRR  
537 289). We thank Thorsten Kahnt for comments and scripts concerning the randomization procedure, Saša Redžepović for  
538 providing scripts used for CS fractal generation, Jürgen Finsterbusch, Katrin Bergholz, Waldemar Schwarz and Kathrin  
539 Wendt for technical assistance during MR data collection, and Alina Schaefer and Jannis Petalas for their assistance with  
540 data collection.

## 541 Author contributions

542 B.H. and C.B. conceived and designed the study, analyzed and interpreted the data, and wrote the manuscript. B.H.  
543 performed the experiments.

## 544 Conflicts of interest

545 The authors declare no competing interests.

## 546 Corresponding author

547 Correspondence should be addressed to Dr. Björn Horing, Department of Systems Neuroscience, University Medical  
548 Center Hamburg-Eppendorf, Martinistrasse 52, 20246 Hamburg, Germany, or via email [b.horing@uke.de](mailto:b.horing@uke.de).

549

## References

1. Seymour B. Pain: A precision signal for reinforcement learning and control. *Neuron*. 2019;101: 1029–1041. doi:10.1016/j.neuron.2019.01.055
2. Trapp S, O’Doherty JP, Schwabe L. Stressful events as teaching signals for the brain. *Trends in Cognitive Sciences*. Elsevier Ltd; 2018. pp. 475–478. doi:10.1016/j.tics.2018.03.007
3. Sutton RS, Barto AG. Reinforcement learning: an introduction. Cambridge: MIT Press; 1998.
4. Rescorla RA, Wagner AR. Classical Conditioning II: Current Research and Theory. In: Black AH, Prokasy WF, editors. New York, NY: Appleton-Century-Crofts; 1972. pp. 64–99.
5. Haarsma J, Fletcher PC, Griffin JD, Taverne HJ, Ziauddeen H, Spencer TJ, et al. Precision weighting of cortical unsigned prediction error signals benefits learning, is mediated by dopamine, and is impaired in psychosis. *Mol Psychiatry*. 2020. doi:10.1038/s41380-020-0803-8
6. Roy M, Shohamy D, Daw N, Jepma M, Wimmer GE, Wager TD. Representation of aversive prediction errors in the human periaqueductal gray. *Nat Neurosci*. 2014;17: 1607–1612. doi:10.1038/nn.3832
7. Yacubian J, Gläscher J, Schroeder K, Sommer T, Braus DF, Büchel C. Dissociable systems for gain- and loss-related value predictions and errors of prediction in the human brain. *J Neurosci*. 2006;26: 9530–9537. doi:10.1523/JNEUROSCI.2915-06.2006
8. Seymour B, Daw N, Dayan P, Singer T, Dolan R. Differential encoding of losses and gains in the human striatum. *J Neurosci*. 2007;27: 4826–4831. doi:10.1523/JNEUROSCI.0400-07.2007
9. Vlaeyen JWS, Kole-Snijders AMJ, Boeren RGB, van Eek H. Fear of movement/(re)injury in chronic low back pain and its relation to behavioral performance. *Pain*. 1995;62: 363–372. doi:10.1016/0304-3959(94)00279-N
10. Rouhani N, Niv Y. Signed and unsigned reward prediction errors dynamically enhance learning and memory. *Elife*. 2021;10. doi:10.7554/eLife.61077
11. Den Ouden HEM, Kok P, de Lange FP. How prediction errors shape perception, attention, and motivation. *Frontiers in Psychology*. *Front Psychol*; 2012. doi:10.3389/fpsyg.2012.00548
12. Geuter S, Boll S, Eippert F, Büchel C. Functional dissociation of stimulus intensity encoding and predictive coding of pain in the insula. *Elife*. 2017;6. doi:10.7554/eLife.24770
13. Kalbe F, Schwabe L. Beyond arousal: Prediction error related to aversive events promotes episodic memory formation. *J Exp Psychol Learn Mem Cogn*. 2020;46: 234–246. doi:10.1037/xlm0000728

- 578 14. Pearce JM, Hall G. A model for Pavlovian learning: Variations in the effectiveness of conditioned but not of  
579 unconditioned stimuli. *Psychol Rev.* 1980;87: 532–552. doi:10.1037/0033-295X.87.6.532
- 580 15. Gershman SJ, Norman KA, Niv Y. Discovering latent causes in reinforcement learning. *Curr Opin Behav Sci.*  
581 2015;5: 43–50. doi:10.1016/j.cobeha.2015.07.007
- 582 16. Roesch MR, Esber GR, Li J, Daw ND, Schoenbaum G. Surprise! Neural correlates of Pearce-Hall and Rescorla-  
583 Wagner coexist within the brain. *Eur J Neurosci.* 2012;35: 1190–1200. doi:10.1111/j.1460-9568.2011.07986.x
- 584 17. Boll S, Gamer M, Gluth S, Finsterbusch J, Büchel C. Separate amygdala subregions signal surprise and  
585 predictiveness during associative fear learning in humans. *Eur J Neurosci.* 2013;37: 758–767.  
586 doi:10.1111/ejn.12094
- 587 18. Le Pelley ME. The role of associative history in models of associative learning: a selective review and a hybrid  
588 model. *Q J Exp Psychol B.* 2004;57: 193–243. doi:10.1080/02724990344000141
- 589 19. Fazeli S, Büchel C. Pain-related expectation and prediction error signals in the anterior insula are not related to  
590 aversiveness. *J Neurosci.* 2018;38: 6461–6474. doi:10.1523/JNEUROSCI.0671-18.2018
- 591 20. Rutledge RB, Dean M, Caplin A, Glimcher PW. Testing the reward prediction error hypothesis with an axiomatic  
592 model. *J Neurosci.* 2010;30: 13525–13536. doi:10.1523/JNEUROSCI.1747-10.2010
- 593 21. Zeidan F, Lobanov O V., Kraft RA, Coghill RC. Brain mechanisms supporting violated expectations of pain. *Pain.*  
594 2015;156: 1. doi:10.1097/j.pain.0000000000000231
- 595 22. Suarez JA, Howard JD, Schoenbaum G, Kahnt T. Sensory prediction errors in the human midbrain signal identity  
596 violations independent of perceptual distance. *Elife.* 2019;8. doi:10.7554/eLife.43962
- 597 23. Howard JD, Kahnt T. Identity prediction errors in the human midbrain update reward-identity expectations in the  
598 orbitofrontal cortex. *Nat Commun.* 2018;9. doi:10.1038/s41467-018-04055-5
- 599 24. Horing B, Sprenger C, Büchel C, Buchel C. The parietal operculum preferentially encodes heat pain and not  
600 salience. *PLoS Biol.* 2019/08/14. 2019;17: e3000205. doi:10.1371/journal.pbio.3000205
- 601 25. Boucsein W. *Electrodermal activity*. 2nd ed. New York: Springer; 2012.
- 602 26. Sequeira H, Hot P, Silvert L, Delplanque S. Electrical autonomic correlates of emotion. *Int J Psychophysiol.*  
603 2009;71: 50–56. doi:10.1016/J.IJPSYCHO.2008.07.009
- 604 27. Kuhn M, Wendt J, Sjouwerman R, Büchel C, Hamm A, Lonsdorf TB. The neurofunctional basis of affective startle  
605 modulation in humans: Evidence from combined facial electromyography and functional magnetic resonance

- 606            imaging. *Biol Psychiatry*. 2020;87: 548–558. doi:10.1016/J.BIOPSYCH.2019.07.028
- 607 28.    Segerdahl AR, Mezue M, Okell TW, Farrar JT, Tracey I. The dorsal posterior insula subserves a fundamental role in  
608 human pain. *Nat Neurosci*. 2015;18: 499–500. doi:10.1038/nn.3969
- 609 29.    Garcia-Larrea L, Peyron R. Pain matrices and neuropathic pain matrices: A review. *Pain*. 2013;154: S29–S43.  
610 doi:10.1016/j.pain.2013.09.001
- 611 30.    Tracey I, Mantyh PW. The cerebral signature for pain perception and its modulation. *Neuron*. 2007;55: 377–391.  
612 doi:10.1016/j.neuron.2007.07.012
- 613 31.    Mazzola L, Isnard J, Peyron R, Mauguière F. Stimulation of the human cortex and the experience of pain: Wilder  
614 Penfield’s observations revisited. *Brain*. 2012;135: 631–640. doi:10.1093/brain/awr265
- 615 32.    Atlas LY, Bolger N, Lindquist MA, Wager TD. Brain mediators of predictive cue effects on perceived pain. *J*  
616 *Neurosci*. 2010;30: 12964–12977. doi:10.1523/JNEUROSCI.0057-10.2010
- 617 33.    NIOSH. Criteria for a Recommended Standard: Occupational Noise Exposure. Revised Criteria. 1998. Available:  
618 <https://www.cdc.gov/niosh/docs/98-126/pdfs/98-126.pdf>
- 619 34.    McGaugh JL. Emotional arousal regulation of memory consolidation. *Current Opinion in Behavioral Sciences*.  
620 Elsevier Ltd; 2018. pp. 55–60. doi:10.1016/j.cobeha.2017.10.003
- 621 35.    Craig a DB. How do you feel--now? The anterior insula and human awareness. *Nat Rev Neurosci*. 2009;10: 59–70.  
622 doi:10.1038/nrn2555
- 623 36.    Allman JM, Tetreault NA, Hakeem AY, Manaye KF, Semendeferi K, Erwin JM, et al. The von Economo neurons in  
624 frontoinsular and anterior cingulate cortex in great apes and humans. *Brain Struct Funct*. 2010;214: 495–517.  
625 doi:10.1007/s00429-010-0254-0
- 626 37.    Uddin LQ, Yeo BTT, Spreng RN. Towards a universal taxonomy of macro-scale functional human brain networks.  
627 *Brain Topogr*. 2019;32: 926. doi:10.1007/S10548-019-00744-6
- 628 38.    Seeley WW, Menon V, Schatzberg AF, Keller J, Glover GH, Kenna H, et al. Dissociable intrinsic connectivity  
629 networks for salience processing and executive control. *J Neurosci*. 2007;27: 2349–2356.  
630 doi:10.1523/JNEUROSCI.5587-06.2007
- 631 39.    Nomi JS, Schettini E, Broce I, Dick AS, Uddin LQ. Structural connections of functionally defined human insular  
632 subdivisions. *Cereb Cortex*. 2018;28: 3445–3456. doi:10.1093/cercor/bhx211
- 633 40.    Ferraro S, Klugah-Brown B, Christopher |, Tench R, Yao S, Nigri A, et al. Dysregulated anterior insula reactivity as

- 634 robust functional biomarker for chronic pain—Meta-analytic evidence from neuroimaging studies. *Hum Brain*  
635 *Mapp.* 2021. doi:10.1002/HBM.25702
- 636 41. Veréb D, Kincses B, Spisák T, Schlitt F, Szabó N, Faragó P, et al. Resting-state functional heterogeneity of the right  
637 insula contributes to pain sensitivity. *Sci Reports* 2021 111. 2021;11: 1–8. doi:10.1038/s41598-021-02474-x
- 638 42. Wiech K, Jbabdi S, Lin CS, Andersson J, Tracey I. Differential structural and resting state connectivity between  
639 insular subdivisions and other pain-related brain regions. *Pain.* 2014;155: 2047–2055.  
640 doi:10.1016/j.pain.2014.07.009
- 641 43. Wiech K, Lin CS, Brodersen KH, Bingel U, Ploner M, Tracey I. Anterior insula integrates information about salience  
642 into perceptual decisions about pain. *J Neurosci.* 2010;30: 16324–16331. doi:10.1523/JNEUROSCI.2087-10.2010
- 643 44. Lang PJ, Greenwald MK, Bradley MM, Hamm AO. Looking at pictures: affective, facial, visceral, and behavioral  
644 reactions. *Psychophysiology.* 1993;30: 261–273. doi:10.1111/J.1469-8986.1993.TB03352.X
- 645 45. Bradley MM, Codispoti M, Cuthbert BN, Lang PJ. Emotion and motivation I: Defensive and appetitive reactions in  
646 picture processing. *Emotion.* 2001;1: 276–298. doi:10.1037/1528-3542.1.3.276
- 647 46. Su L, Zulfiqar I, Jamshed F, Fonteneau E, Marslen-Wilson W. Mapping tonotopic organization in human temporal  
648 cortex: representational similarity analysis in EMEG source space. *Front Neurosci.* 2014;8: 368.  
649 doi:10.3389/fnins.2014.00368
- 650 47. Brewer AA, Barton B. Maps of the Auditory Cortex. *Annu Rev Neurosci.* 2016;39: 385–407. doi:10.1146/annurev-  
651 neuro-070815-014045
- 652 48. Bastuji H, Frot M, Perchet C, Hagiwara K, Garcia-Larrea L. Convergence of sensory and limbic noxious input into  
653 the anterior insula and the emergence of pain from nociception. *Sci Rep.* 2018;8: 13360. doi:10.1038/s41598-  
654 018-31781-z
- 655 49. Jepma M, Roy M, Ramlakhan K, Velzen M van, Dahan A. Different brain systems support the aversive and  
656 appetitive sides of human pain-avoidance learning. *bioRxiv.* 2021; 2021.10.18.464769.  
657 doi:10.1101/2021.10.18.464769
- 658 50. Mumford JA, Poline JB, Poldrack RA. Orthogonalization of regressors in fMRI models. *PLoS One.* 2015;10.  
659 doi:10.1371/journal.pone.0126255
- 660 51. Hemington KS, Wu Q, Kucyi A, Inman RD, Davis KD. Abnormal cross-network functional connectivity in chronic  
661 pain and its association with clinical symptoms. *Brain Struct Funct.* 2016;221: 4203–4219. doi:10.1007/s00429-  
662 015-1161-1

- 663 52. Beck AT, Steer RA, Brown GK. Manual for the Beck Depression Inventory-II. San Antonio, TX: Psychological  
664 Corporation Press; 1996.
- 665 53. Kroenke K, Spitzer RL, Williams JBW. The PHQ-15: Validity of a new measure for evaluating the severity of  
666 somatic symptoms. *Psychosom Med.* 2002;64: 258–266. doi:10.1097/00006842-200203000-00008
- 667 54. Rolke R, Magerl W, Campbell KA, Schalber C, Caspari S, Birklein F, et al. Quantitative sensory testing: A  
668 comprehensive protocol for clinical trials. *Eur J Pain.* 2006;10: 77–88. doi:10.1016/j.ejpain.2005.02.003
- 669 55. Benedek M, Kaernbach C. A continuous measure of phasic electrodermal activity. *J Neurosci Methods.* 2010;190:  
670 80–91. doi:10.1016/J.JNEUMETH.2010.04.028
- 671 56. D’Hondt F, Lassonde M, Collignon O, Dubarry A-S, Robert M, Rigoulot S, et al. Early brain-body impact of  
672 emotional arousal. *Front Hum Neurosci.* 2010;4: 33. doi:10.3389/fnhum.2010.00033
- 673 57. Critchley HD. Review: Electrodermal responses: What happens in the brain. *Neurosci.* 2002;8: 132–142.  
674 doi:10.1177/107385840200800209
- 675 58. Loggia ML, Juneau M, Bushnell MC. Autonomic responses to heat pain: Heart rate, skin conductance, and their  
676 relation to verbal ratings and stimulus intensity. *Pain.* 2011;152: 592–598. doi:10.1016/j.pain.2010.11.032
- 677 59. Bach DR, Flandin G, Friston KJ, Dolan RJ. Modelling event-related skin conductance responses. *Int J*  
678 *Psychophysiol.* 2010;75: 349–356. doi:10.1016/J.IJPSYCHO.2010.01.005
- 679 60. Cousineau D, O’Brien F. Error bars in within-subject designs: a comment on Baguley (2012). *Behavior research*  
680 *methods.* *Behav Res Methods;* 2014. pp. 1149–1151. doi:10.3758/s13428-013-0441-z
- 681 61. Fan L, Li H, Zhuo J, Zhang Y, Wang J, Chen L, et al. The Human Brainnetome Atlas: A new brain atlas based on  
682 connectional architecture. *Cereb Cortex.* 2016;26: 3508–3526. doi:10.1093/cercor/bhw157
- 683

## Supporting information

for

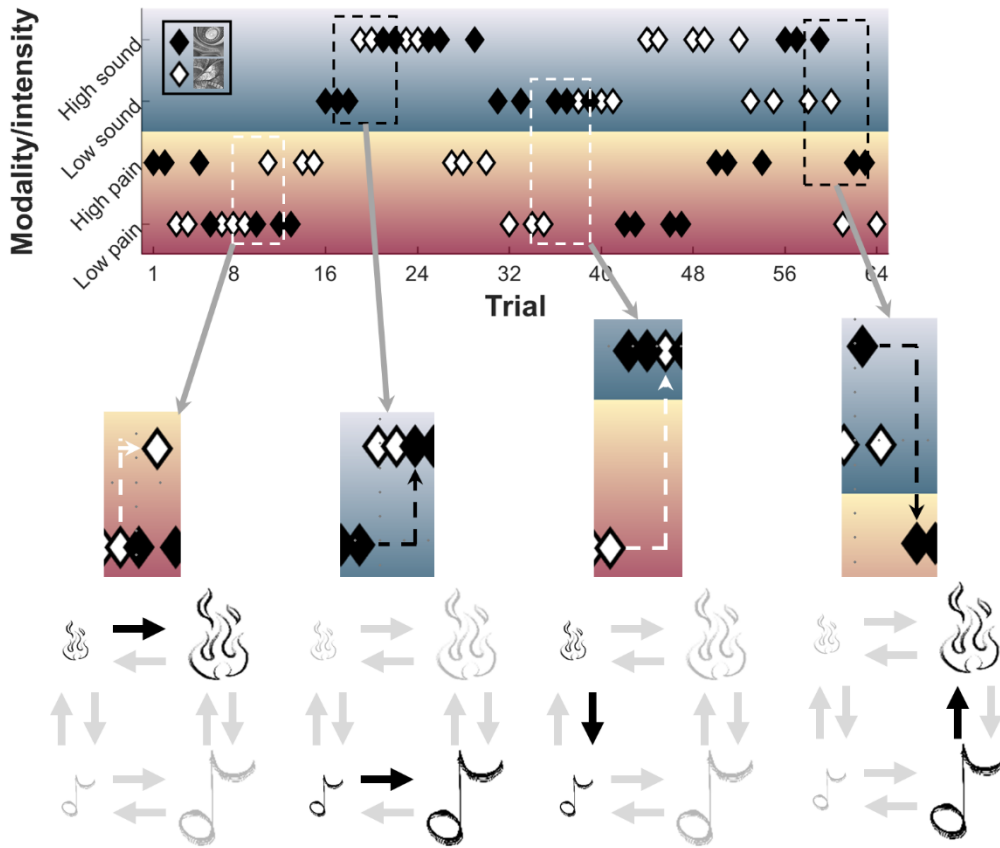
## Pain-related learning signals in the human insula

Björn Horing\* & Christian Büchel

Affective Neuroscience Group, Department of Systems Neuroscience, University Medical Center Hamburg-Eppendorf,  
22303 Hamburg, Germany

\*Corresponding author, e-mail [b.horing@uke.de](mailto:b.horing@uke.de)

693	<b>Supporting Figure 1.</b> Illustration of reversal types.....	2
694	<b>Supporting Figure 2.</b> Behavioral results for low and high unconditioned pain and sound stimuli.....	3
695	<b>Supporting Figure 3.</b> Results from skin conductance response measurements, by prediction error type. ....	4
696	<b>Supporting Figure 4.</b> Lateral and medial views of brain surface results for heat and sound onsets.....	5
697	<b>Supporting Figure 5.</b> Brain volume results for heat and sound onsets.....	6
698	<b>Supporting Figure 6.</b> Lateral and medial views of brain surface results for pain and sound ratings.....	7
699	<b>Supporting Figure 7.</b> Brain volume results for pain and sound ratings.....	8
700	<b>Supporting Figure 8.</b> Lateral and medial views of brain surface results for unsigned intensity prediction errors.....	9
701	<b>Supporting Figure 9.</b> Brain volume results for unsigned intensity prediction errors.....	10
702	<b>Supporting Figure 10.</b> Lateral and medial views of brain surface results for modality prediction errors.....	11
703	<b>Supporting Figure 11.</b> Brain volume results for modality prediction errors.....	12
704	<b>Supporting Figure 12.</b> Lateral and medial views of brain surface results for signed intensity prediction errors.....	13
705	<b>Supporting Figure 13.</b> Brain volume results of signed intensity prediction errors.....	14
706	<b>Supporting Figure 14.</b> Mean performance split by modality/intensity.....	15
707		
708	<b>Supporting Table 1.</b> Effects of modality and intensity, by prediction error type.....	5
709	<b>Supporting Table 2.</b> Sample characteristics.....	16
710		
711	<b>Supporting References</b> .....	17



712

713

**Supporting Figure 1.** Illustration of reversal types. Both conditioned stimuli have an independent sequence of deterministic associations with one of the four unconditioned stimuli (also see Figure 2). The dashed lines illustrate reversals for CS1 (black) or CS2 (white). First column, CS2 intensity reversal from low to high heat; second column, CS1 intensity reversal from low to high sound; third column, CS2 modality reversal from low heat to low sound; fourth column, modality reversal from high sound to high heat.

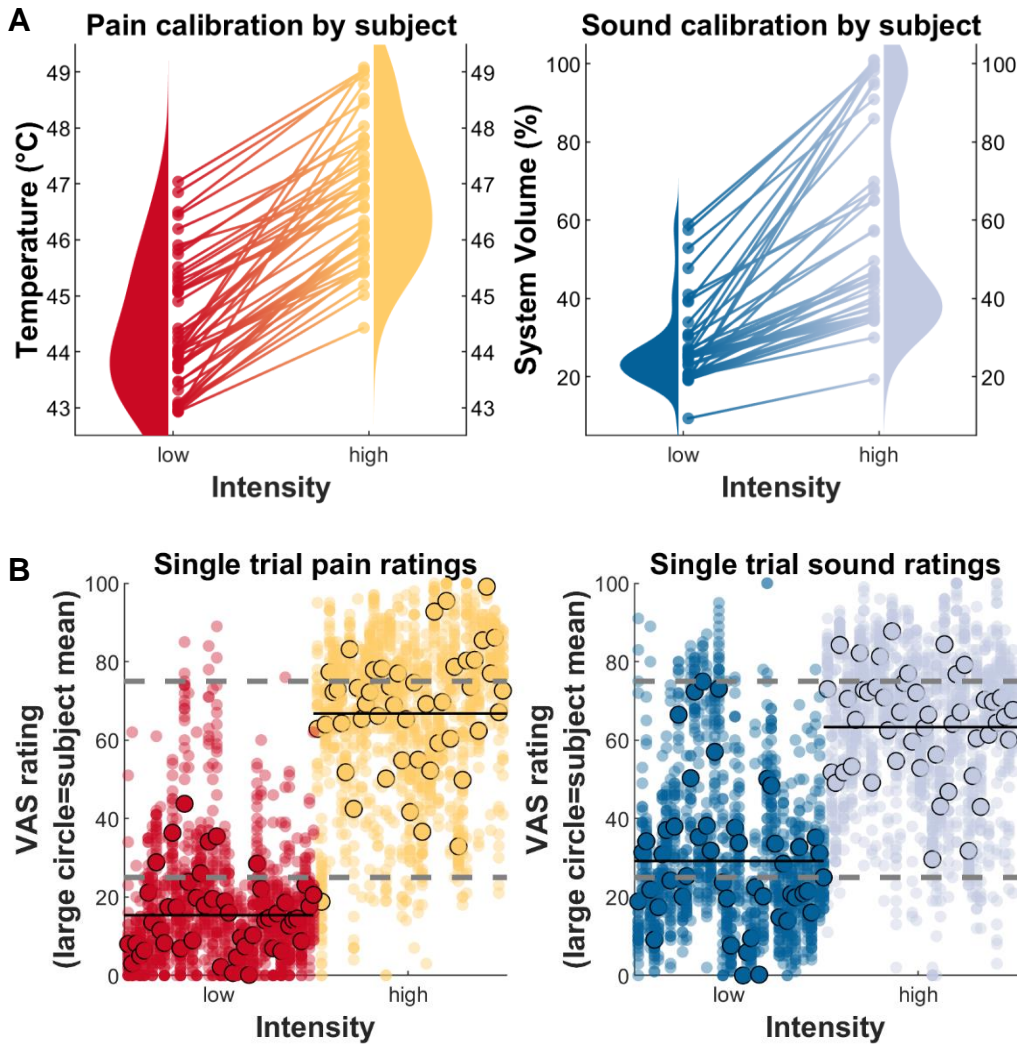
717

718

719

720





721

722

723

724

725

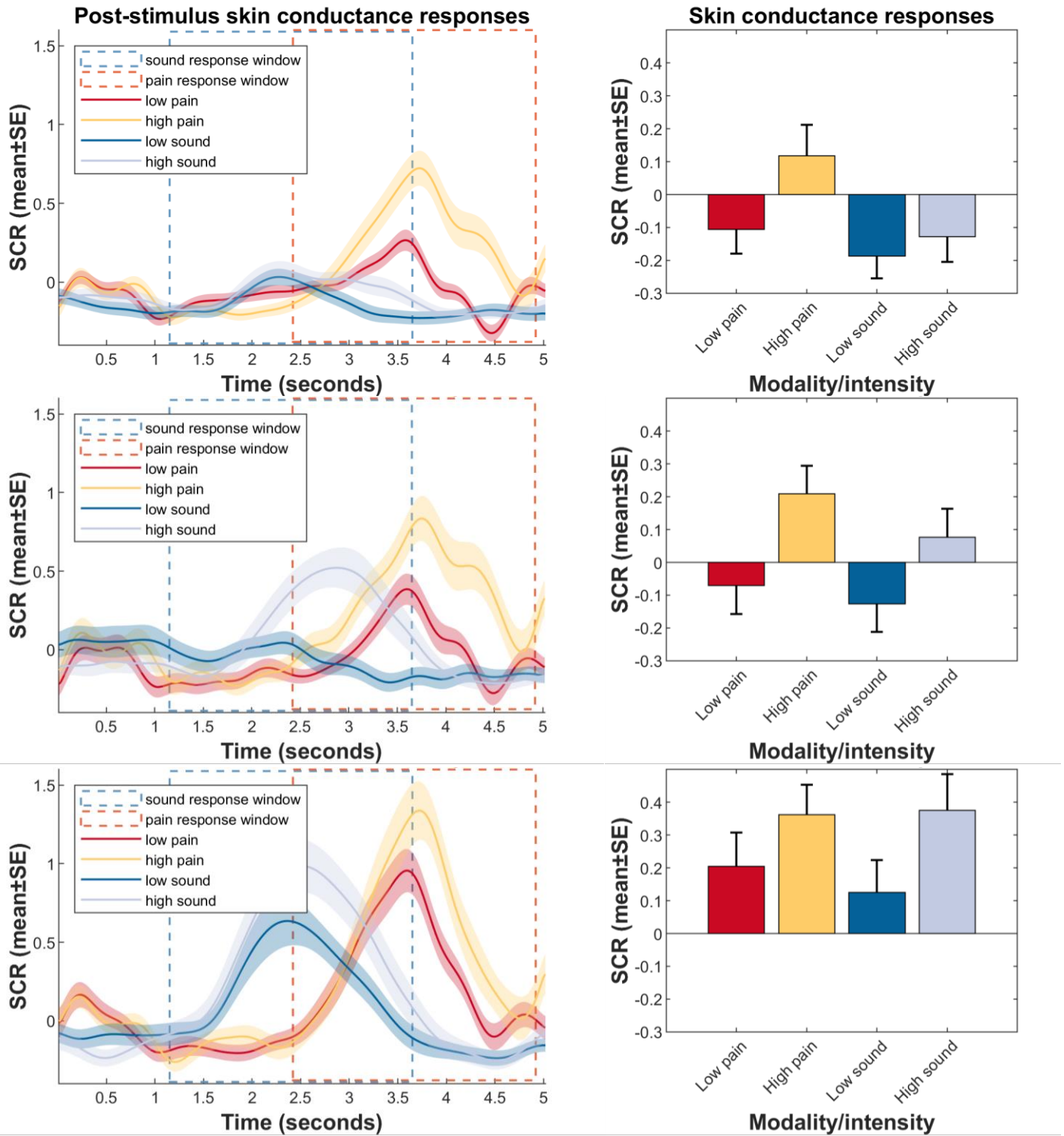
726

727

728

729

**Supporting Figure 2.** Behavioral results for low and high unconditioned pain and sound stimuli. **(A)** Calibrated stimulus intensities corresponding to VAS25 (low intensity) and VAS75 (high intensity) for pain stimuli and sound stimuli. Each line represents the two intensities per modality per subject; the violin plots aggregate over subjects. **(B)** Single trial ratings following pain stimulation and sound stimulation. Every column represents a single subject's response to the respective intensity and modality; the bordered circle is a subject's mean rating. The grey dashed lines is the "intended" rating as per calibration (VAS25 for low, VAS75 for high intensities). The black line is the actual mean rating over all subjects.



**Supporting Figure 3.** Results from skin conductance response measurements, by prediction error type. Rows show group means of SCR following no prediction error (row 1), intensity PE (row 2), and modality PE (row 3). Column show post-stimulus SCR (left) and SCR averaged within the indicated response windows (right). Differences between conditions are largest in the no PE condition, smallest in the modality PE condition, which also shows the largest SCR amplitudes. Statistics of differences between conditions are displayed in Supporting Table 1. All plots are based on log- and z-transformed data.

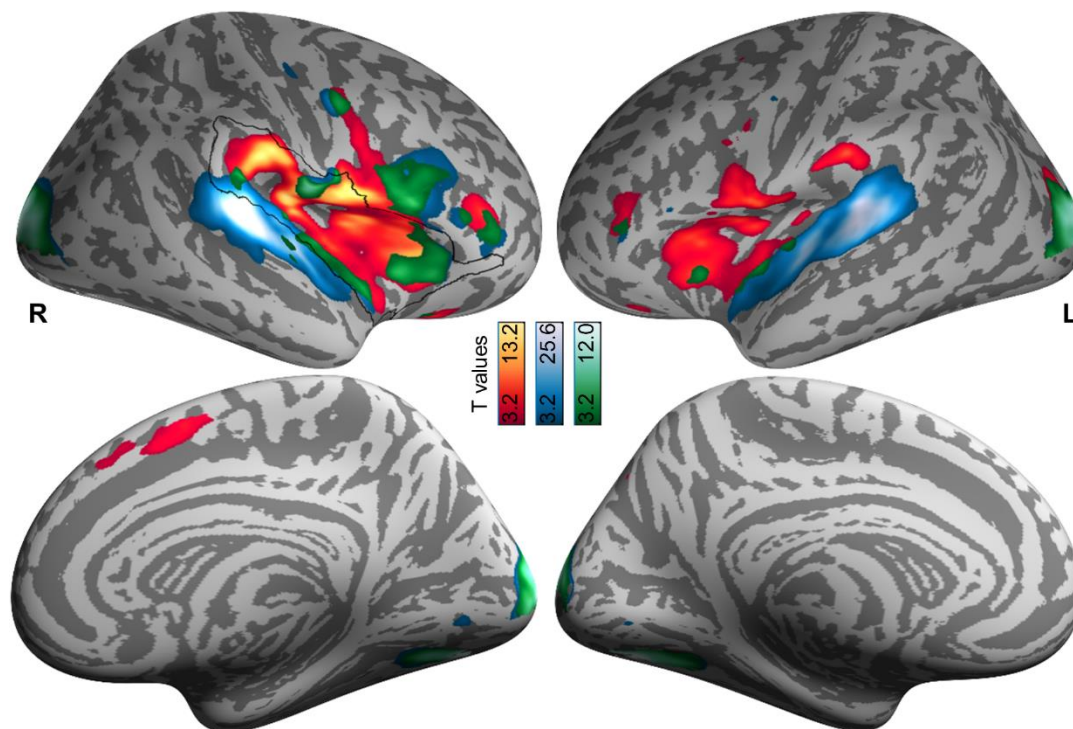
738  
739  
740

**Supporting Table 1.** Effects of modality and intensity, by prediction error type. Parameters obtained from linear mixed models with random subject intercept. Differences between the conditions are largest in trials with no prediction error, and smallest in trials with modality prediction error (cf. Supporting Figure 1).

Subanalysis	Term	Estimate	SE	CI Lower	CI Upper	p
No prediction error	Modality	-0.0442	0.0307	-0.1044	0.0161	0.1506
	Intensity	0.2444	0.0305	0.1845	0.3042	$2 \times 10^{-15}$ *
	Modality*Intensity	-0.2023	0.0433	-0.2873	-0.1173	$3 \times 10^{-6}$ *
Intensity prediction error	Modality	-0.0506	0.0603	-0.1689	0.0677	0.4014
	Intensity	0.2479	0.0598	0.1305	0.3653	$4 \times 10^{-5}$ *
	Modality*Intensity	-0.026	0.0838	-0.1904	0.1385	0.7566
Modality prediction error	Modality	-0.056	0.0698	-0.1929	0.0809	0.4227
	Intensity	0.1138	0.071	-0.0257	0.2532	0.1096
	Modality*Intensity	0.0973	0.0994	-0.0977	0.2924	0.3277

741  
742

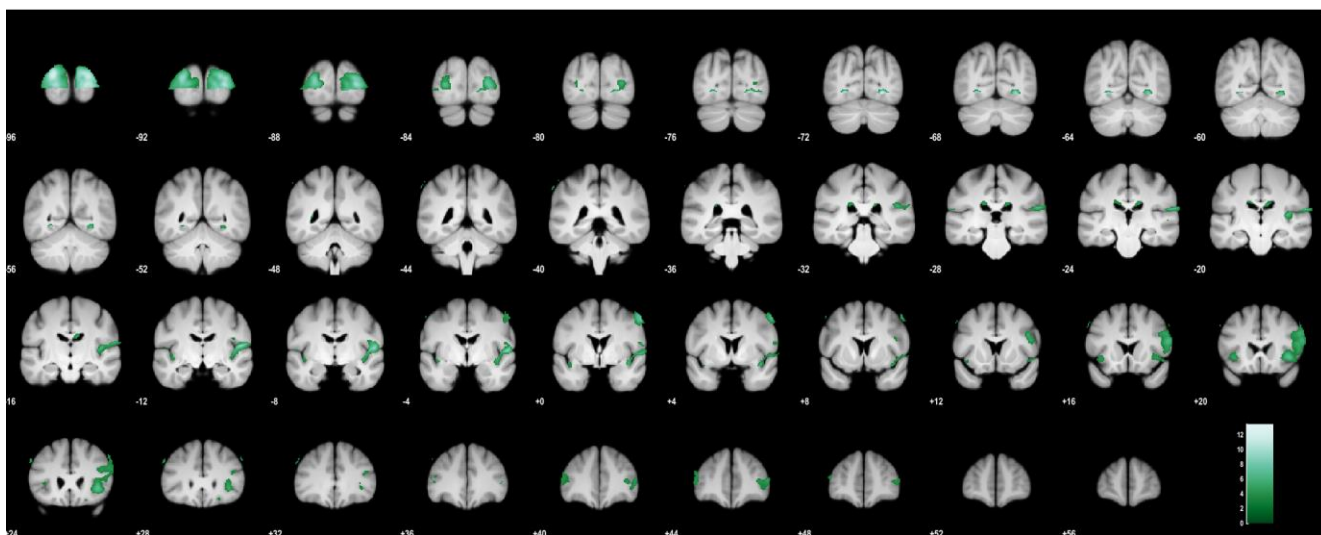
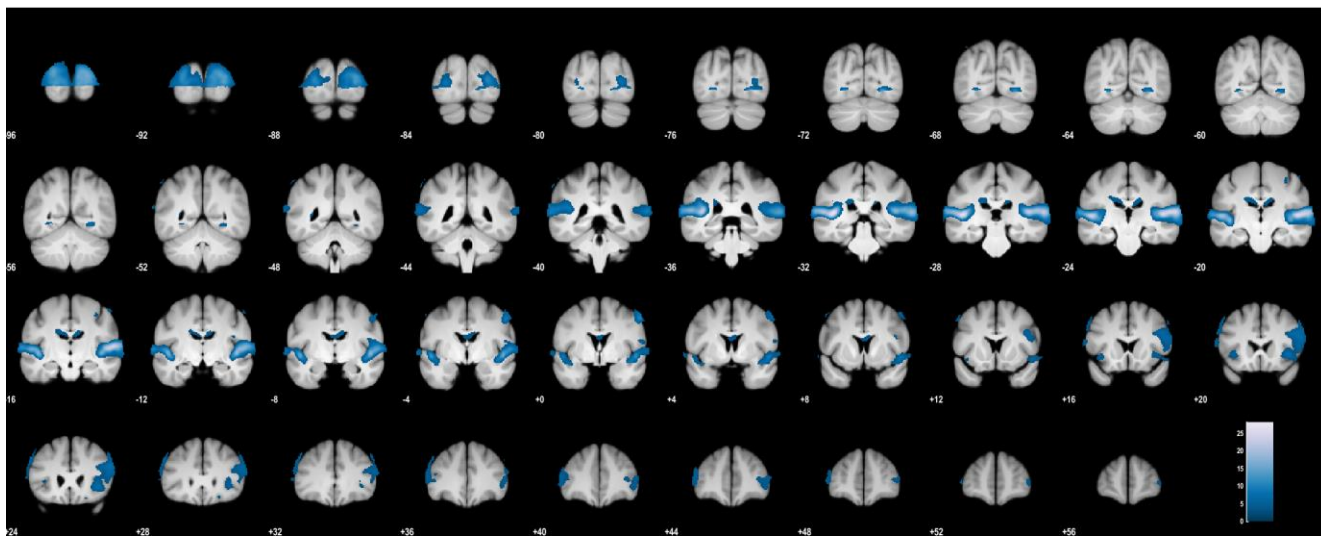
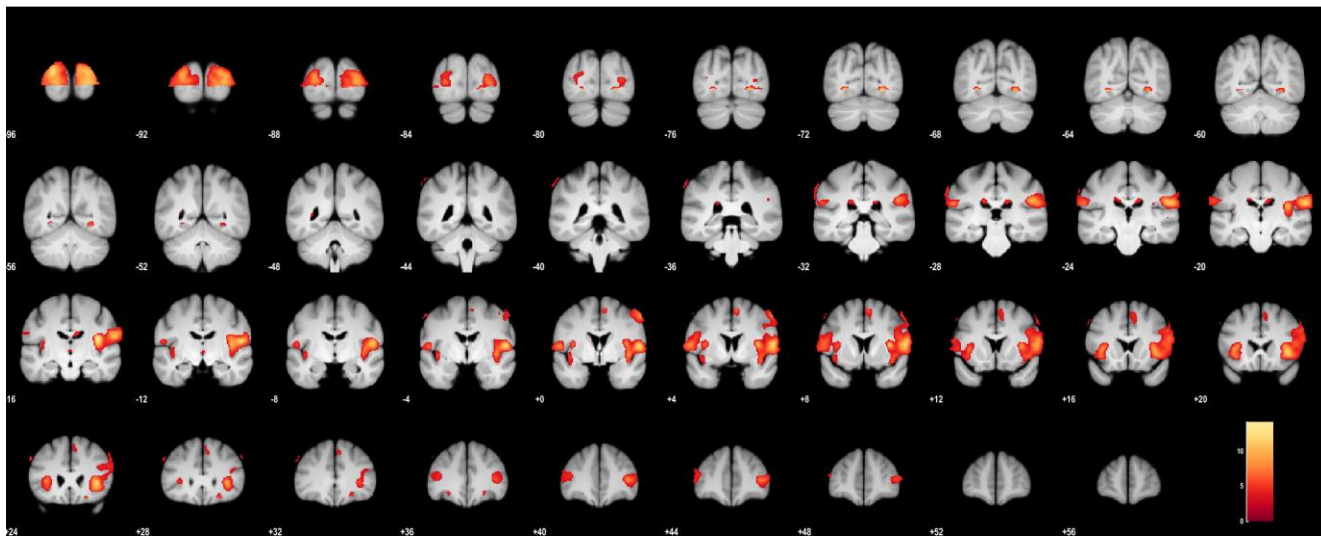
\*p < 0.001.



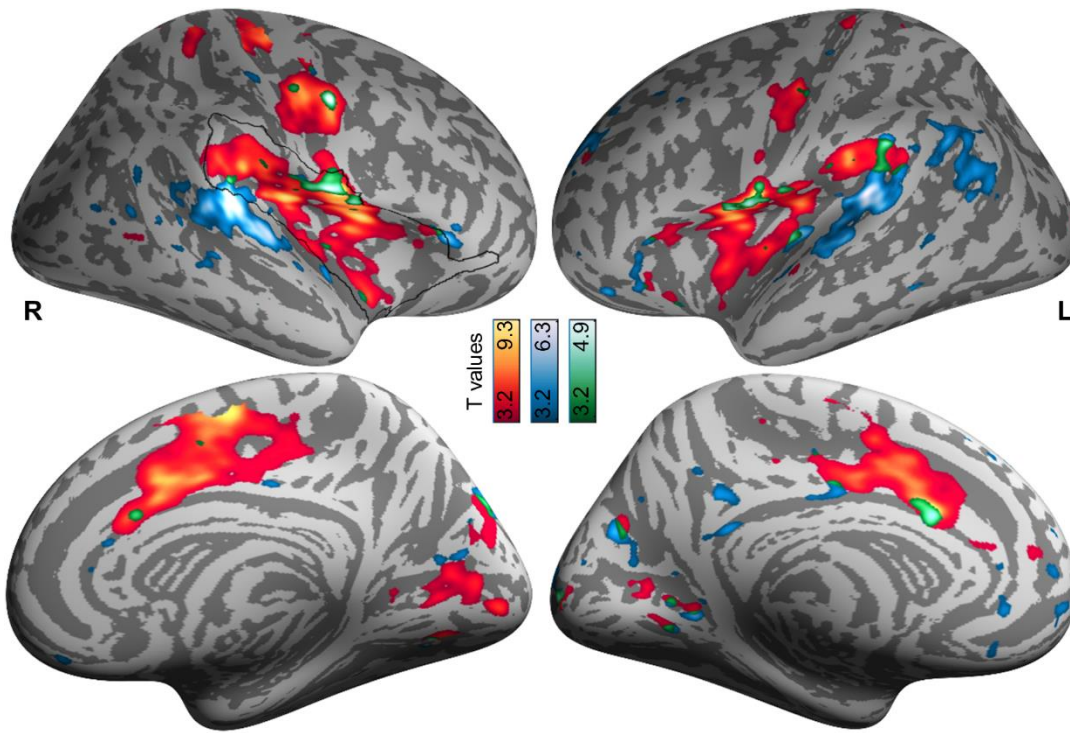
743

744  
745  
746

**Supporting Figure 4.** Lateral and medial views of brain surface results for heat onsets (yellow/red), sound onsets (blue), and their conjunction (green). Activations are overlaid on an average brain surface and thresholded at  $p[\text{uncorr.}] < 0.001$ . The black line delineates the region of interest whose results are highlighted in Figure 5a/b. R, right hemisphere; L, left hemisphere.

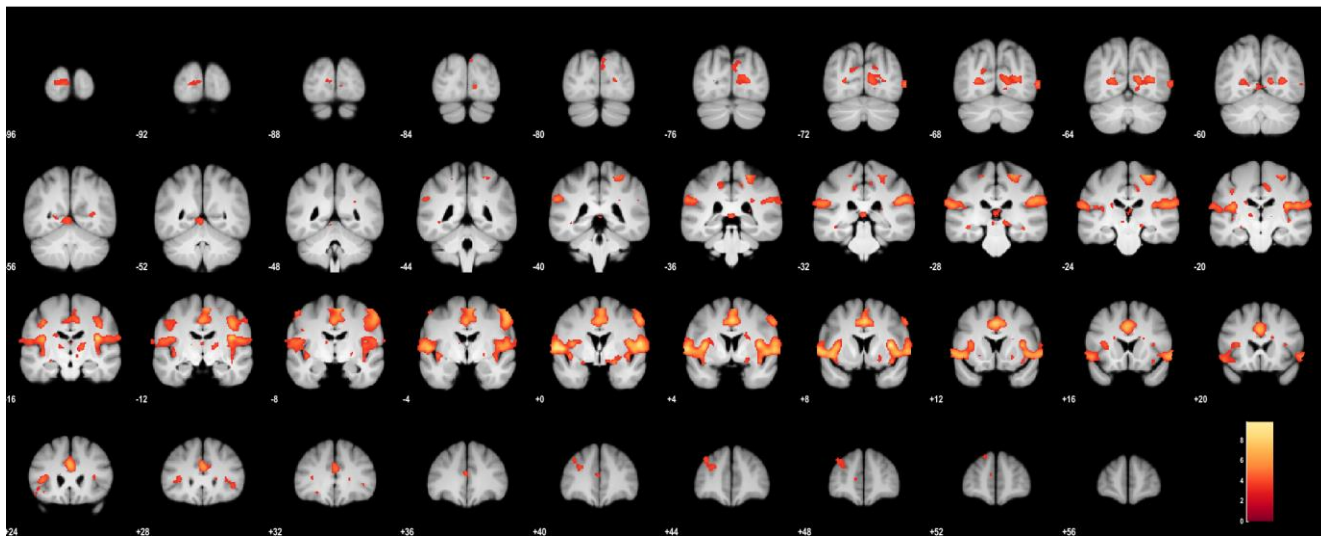


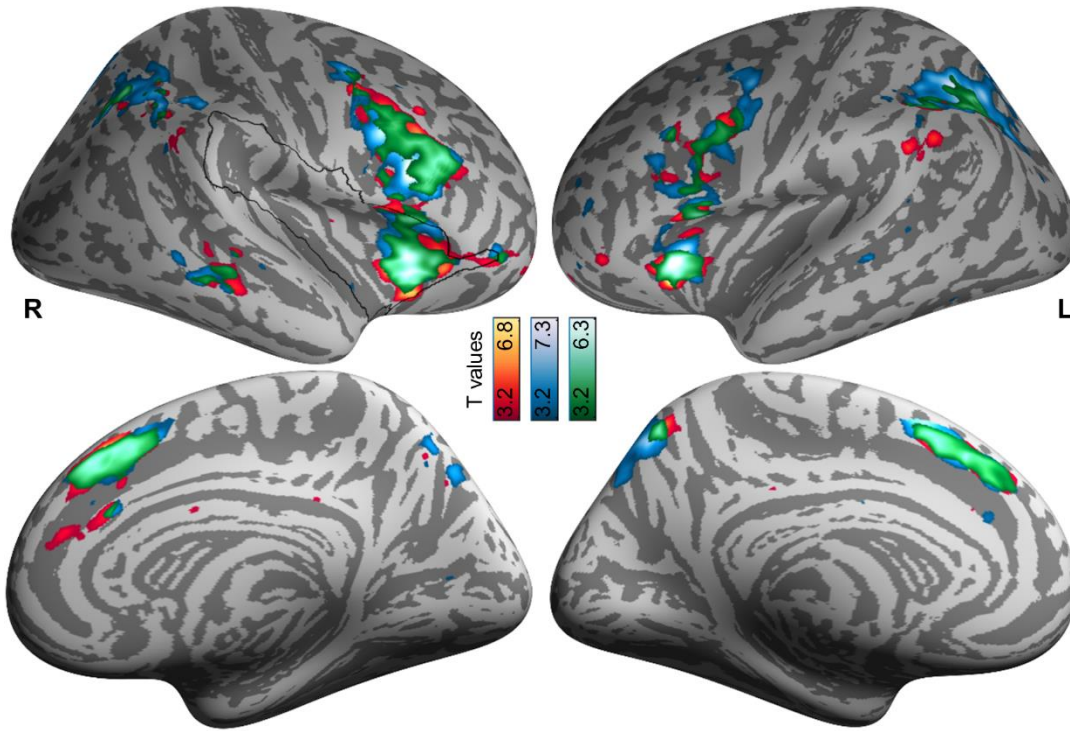
750 **Supporting Figure 5.** Brain volume results for heat onsets (yellow/red), sound onsets (blue), and their conjunction (green).  
751 Activations are overlaid on an average brain volume and thresholded at  $p[\text{uncorr.}] < 0.001$ .



752

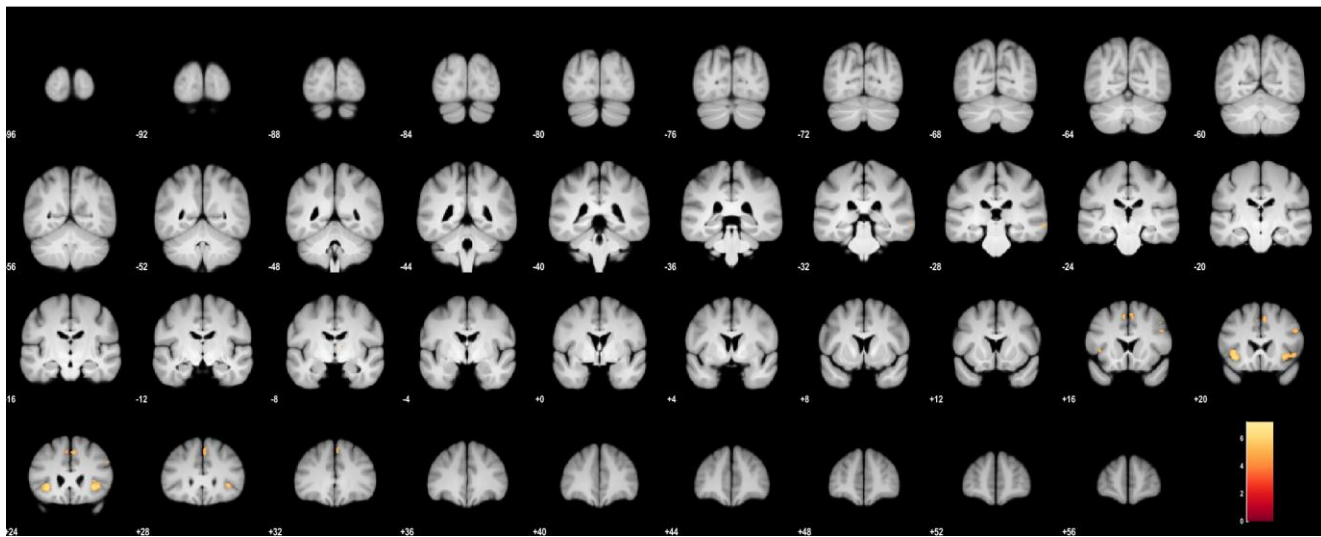
753 **Supporting Figure 6.** Lateral and medial views of brain surface results for pain ratings (yellow/red), sound ratings (blue), and their  
754 conjunction (green). Activations are overlaid on an average brain surface and thresholded at  $p[\text{uncorr.}] < 0.001$ . The black line  
755 delineates the region of interest whose results are highlighted in Figure 5b/c. R, right hemisphere; L, left hemisphere.  
756



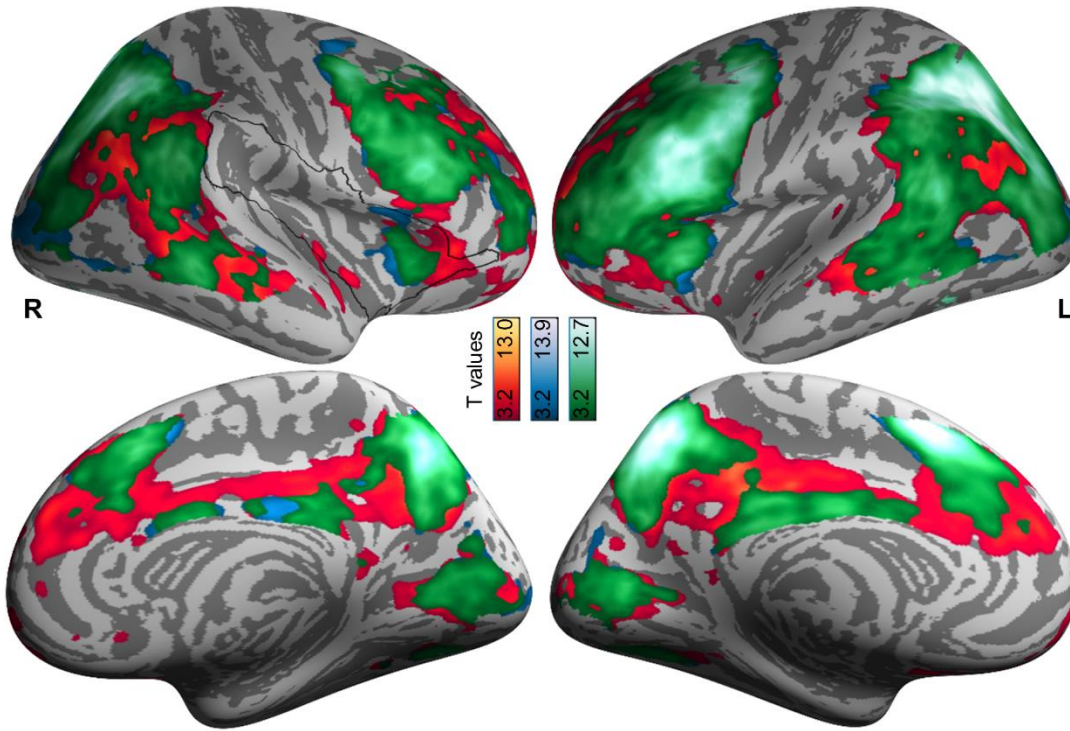


762

763 **Supporting Figure 8.** Lateral and medial views of brain surface results for unsigned intensity prediction errors for heat (yellow/red),  
764 sound (blue), and their conjunction (green). Activations are overlaid on an average brain surface and thresholded at  $p[\text{uncorr.}] <$   
765  $0.001$ . The black line delineates the region of interest whose results are highlighted in Figure 6. R, right hemisphere; L, left  
766 hemisphere.  
767







773

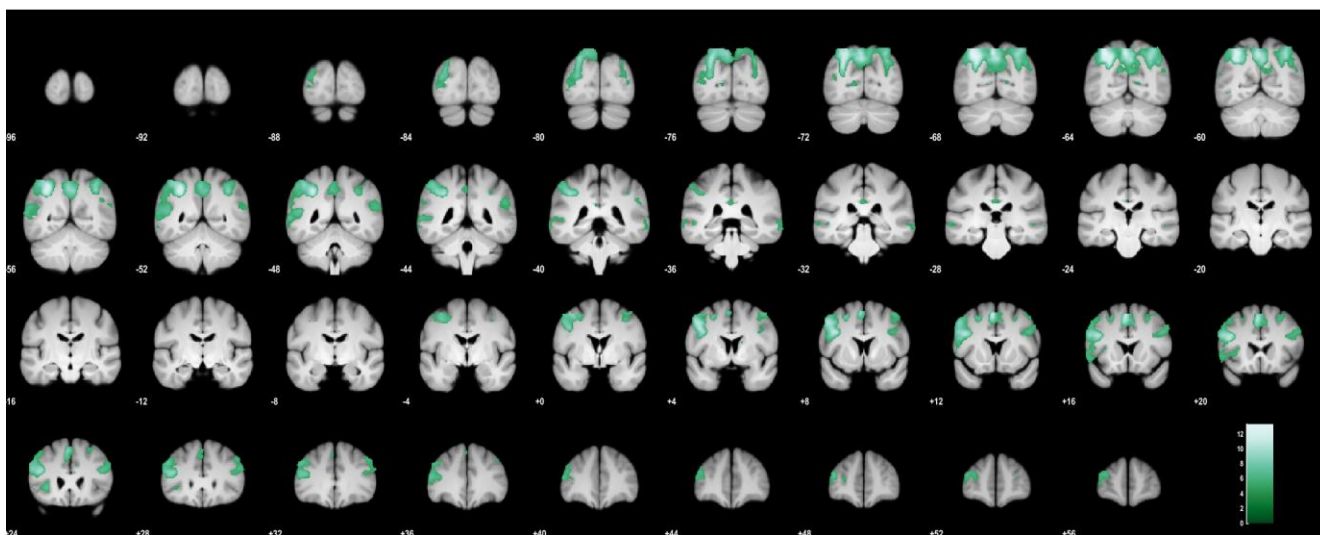
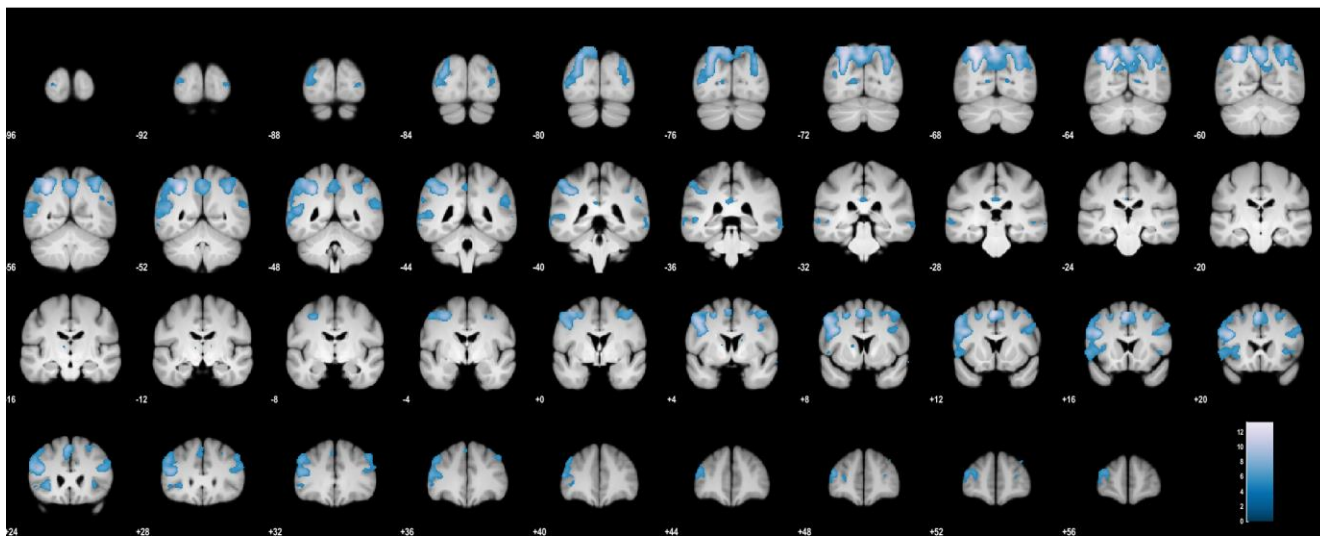
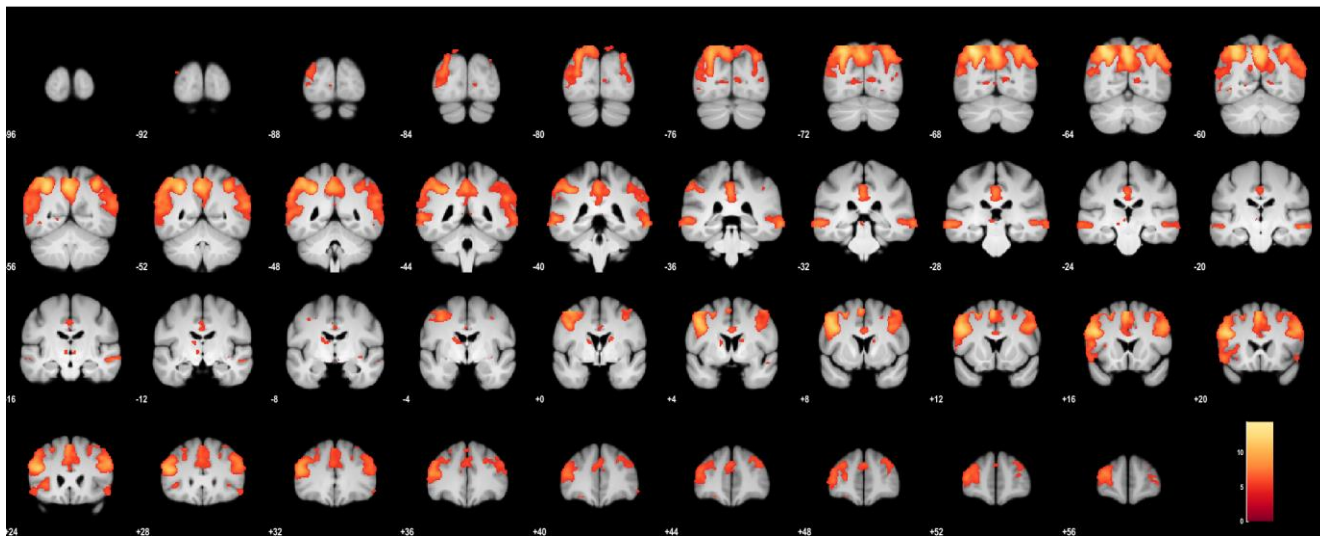
774

775

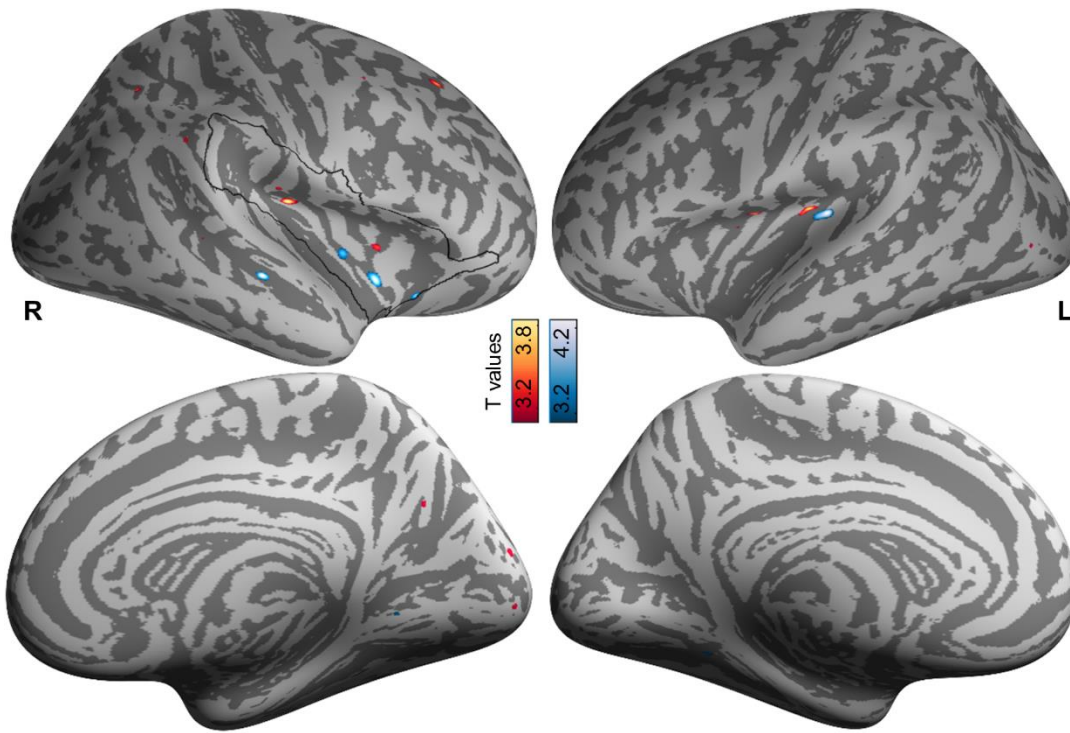
776

777

**Supporting Figure 10.** Lateral and medial views of brain surface results for modality prediction errors for heat (yellow/red), sound (blue), and their conjunction (green). Activations are overlaid on an average brain surface and thresholded at  $p[\text{uncorr.}] < 0.001$ . The black line delineates the region of interest whose results are highlighted in Figure 7. R, right hemisphere; L, left hemisphere.

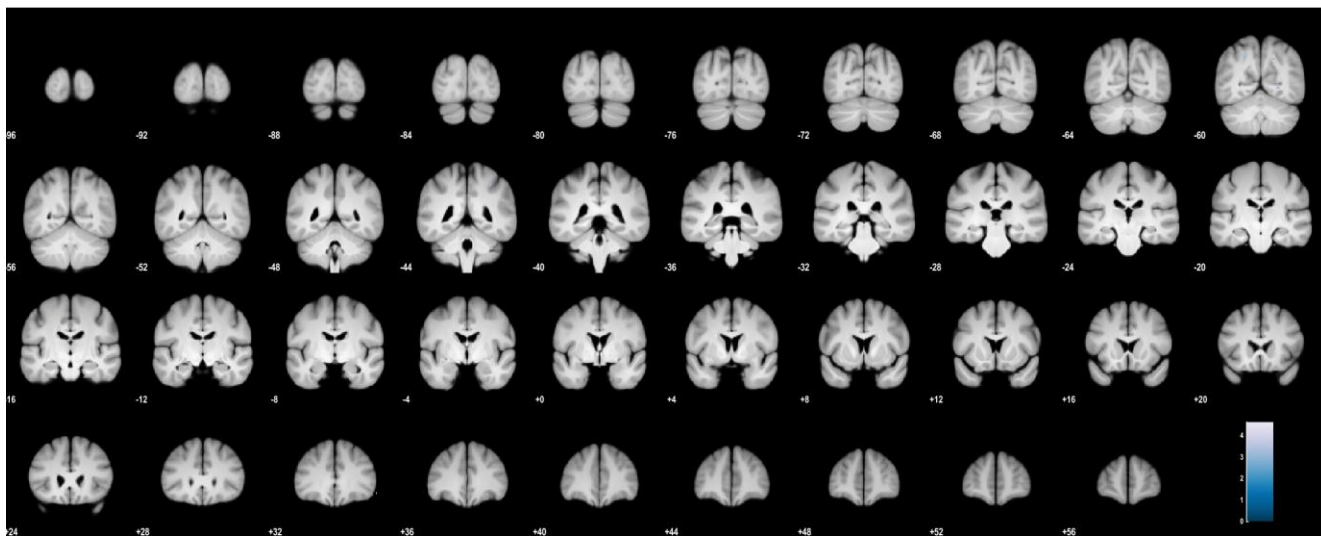
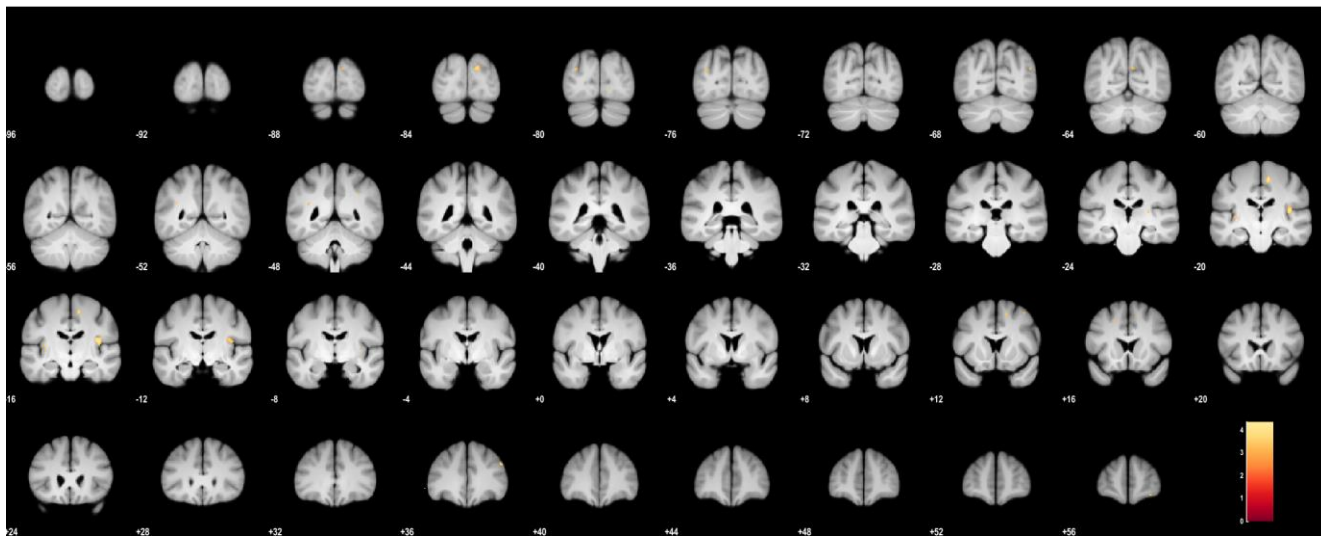


781 **Supporting Figure 11.** Brain volume results for modality prediction errors for heat (yellow/red), sound (blue), and their conjunction  
782 (green). Activations are overlaid on an average brain volume and thresholded at  $p[\text{uncorr.}] < 0.001$ .



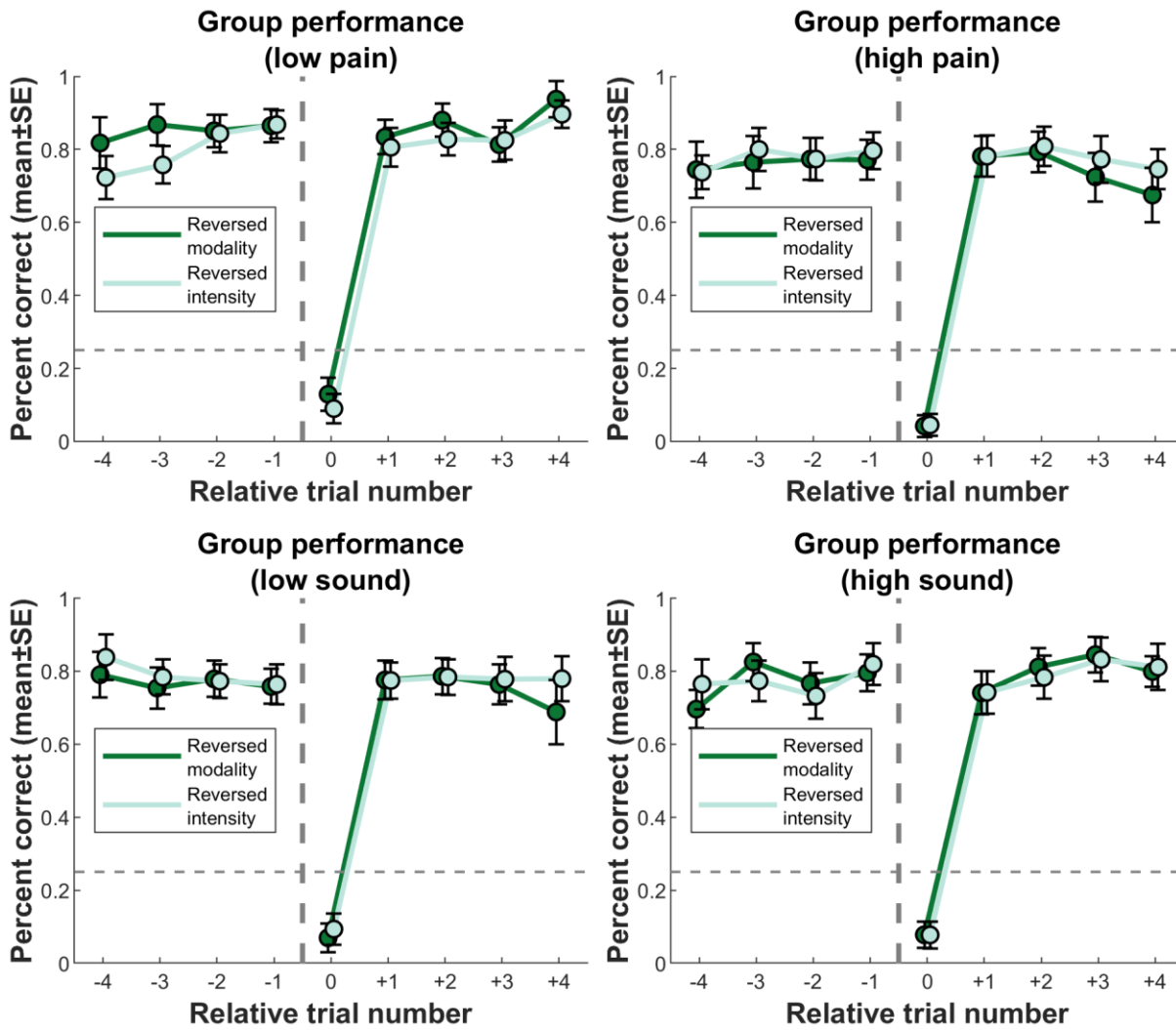
783

784 **Supporting Figure 12.** Lateral and medial views of brain surface results for signed intensity prediction errors for heat (yellow/red)  
785 and sound (blue). No significant conjunction activation prevails. Activations are overlaid on an average brain surface and thresholded  
786 at  $p[\text{uncorr.}] < 0.001$ . The black line delineates the region of interest whose results are highlighted in Figure 9. R, right hemisphere; L,  
787 left hemisphere.  
788



791 **Supporting Figure 13.** Brain volume results of signed intensity prediction errors for heat (yellow/red) and sound (blue). No  
792 significant conjunction activation prevails. Activations are overlaid on an average brain volume and thresholded at  $p[\text{uncorr.}] <$   
793 0.001.

794



795

796

**Supporting Figure 14.** Mean performance split by modality/intensity. Grand mean performance is shown in Figure 3b.

797

798

799  
800  
801  
802

**Supporting Table 2.** Sample characteristics. For references, see Supporting References. BDI-II, Beck Depression Inventory II; PHQ15, Patient Health Questionnaire-15; FPQ, Fear of Pain Questionnaire; PVAQ, Pain Vigilance and Awareness Questionnaire; PSQ, Pain Sensitivity Questionnaire; PRSS, Pain-Related Self-Statements; STAI, State-Trait Anxiety Inventory; MDMQ, Multidimensional Mood Questionnaire; exp., experiment.

Questionnaire	Construct	Mean±SD	Sample range	Possible range
<b>BDI-II</b> [SR 1,2]	Depression	4.0±3.7	0-13	0-63
<b>PHQ15</b> [SR 3]	Somatization	3.4±2.7	0-10	0-30
<b>FPQ</b> [SR 4]				
severe	Fear of pain	29.9±9.6	10-50	10-50
minor	Fear of pain	16.3±5.2	10-34	10-50
<b>PVAQ</b> [SR 5]	Pain vigilance and awareness	36.2±9.9	9-63	0-80
<b>PSQ</b> [SR 6]	Pain sensitivity	43.3±16.0	9-80	0-140
<b>PRSS</b> [SR 7]				
Catastrophizing	Pain catastrophizing	8.4±6.1	1-27	0-45, higher more catastrophizing
Coping	Pain coping	31.3±6.0	19-43	0-45, higher more active coping
<b>STAI</b> [SR 8,9]				
Trait	Trait anxiety	33.1±5.9	23-48	20-80
State	State anxiety (pre experiment)	33.4±6.2	23-49	20-80
<b>MDMQ</b> [SR 10]				
GoodBad A	Mood: Good vs bad (pre exp.)	17.3±2.0	12-20	4-24, the higher the better mood
AwakeTired A	Mood: Awake vs tired (pre exp.)	14.5±2.9	8-20	4-24, the higher the more awake
CalmNervous A	Mood: Calm vs nervous (pre exp.)	16.1±2.2	10-20	4-24, the higher the calmer
GoodBad B	Mood: Good vs bad (post exp.)	17.2±2.0	11-20	4-24, the higher the better mood
AwakeTired B	Mood: Awake vs tired (post exp.)	11.7±3.1	7-18	4-24, the higher the more awake
CalmNervous B	Mood: Calm vs nervous (post exp.)	17.2±2.4	11-20	4-24, the higher the calmer

803

## 804 Supporting References

- 805 SR 1. Beck AT, Steer RA, Brown GK. Manual for the Beck Depression Inventory-II. San Antonio, TX: 810 Psychological  
806 Corporation Press; 1996. 811
- 807 SR 2. Hautzinger M, Keller F, Kühner C. BDI-II. Beck-Depressions-Inventar. Revision. 2nd ed. 812 Frankfurt: Pearson  
808 Assessment; 2009. 813
- 809 SR 3. Kroenke K, Spitzer RL, Williams JBW. The PHQ-15: validity of a new measure for evaluating the 814 severity of  
810 somatic symptoms. *Psychosom Med.* 2002;64(2):258–66. 815
- 811 SR 4. McNeil DW, Rainwater AJ. Development of the Fear of Pain Questionnaire-III. *J Behav Med.* 816 1998;21(4):389–  
812 410. 817
- 813 SR 5. McCracken LM. "Attention" to pain in persons with chronic pain: A behavioral approach. 818 *Behav Ther.*  
814 1997;28(2):271–84. doi: 10.1016/S0005-7894(97)80047-0 819
- 815 SR 6. Ruscheweyh R, Marziniak M, Stumpfenhorst F, Reinholz J, Knecht S. Pain sensitivity can be 820 assessed by self-  
816 rating: Development and validation of the Pain Sensitivity Questionnaire. 821 *Pain.* 2009;146(1):65–74. doi:  
817 10.1016/j.pain.2009.06.020 822
- 818 SR 7. Flor H, Behle DJ, Birbaumer N. Assessment of pain-related cognitions in chronic pain patients. 823 *Behav Res*  
819 *Ther.* 1993;31(1):63–73. 824
- 820 SR 8. Spielberger CD, Gorsuch RL, Lushene RE. Manual for the State-Trait Anxiety Inventory. Palo 825 Alto, CA:  
821 Consulting Psychologists Press; 1970. 826
- 822 SR 9. Laux L, Glanzmann P, Schaffner P, Spielberger CD. Das State-Trait-Angstinventar. Weinheim: 827 Beltz; 1981. 828
- 823 SR 10. Steyer R, Schwenkmezger P, Notz P, Eid M. Der Mehrdimensionale Befindlichkeitsfragebogen 829 (MDBF).  
824 Handanweisung. Göttingen: Hogrefe; 1997.